Nanoscale

Accepted Manuscript

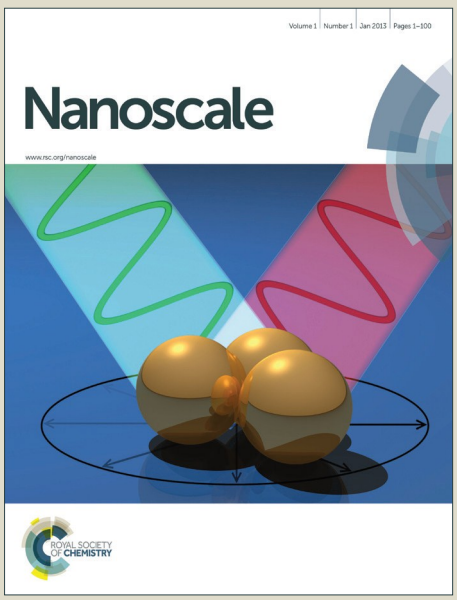

ROYAL SOCIETY OF CHEMISTRY

www.rsc.org/nanoscale

Submitted to *Nanoscale*, July 2015 (Revised October 2015)

Silicon as Potential Anode Material for Li-ion Batteries: Where Size, Geometry and Structure Matter

Maziar Ashuri [a, b], Qianran He [a, b], Leon L. Shaw [a, b, *]

[a] Department of Mechanical, Materials and Aerospace Engineering
Illinois Institute of Technology, Chicago, IL, USA

[b] Wanger Institute for Sustainable Energy Research (WISER)
Illinois Institute of Technology, Chicago, IL, USA

Abstract

Silicon has gained a huge attention in the last decade because it has a theoretical capacity ~10 times higher than that of graphite. However, the practical application of Si is hindered by three major challenges: large volume expansion during cycling (~300%), low electrical conductivity, and instability of the SEI layer caused by repeated volume change of the Si material. Enormous research efforts have been devoted to addressing these challenges and significant breakthroughs have been made particularly in the last two years (2014 and 2015). In this review, we have focused on the principles of Si material designs, novel synthesis methods to achieve such structural designs, and synthesis-structure-performance relationships to enhance the properties of Si anodes. To provide a systematic overview of the Si material design strategies, we have grouped the design strategies into several categories, including (i) particle-based structures (containing nanoparticles, solid core-shell structure, hollow core-shell structure, and yolk-shell structure), (ii) porous Si designs, (iii) nanowires, nanotubes and nanofibers, (iv) Si-based composites, and (v) unusual designs. Finally, personal perspectives on outlook are offered with an aim to stimulate further discussion and ideas in the rational design of durable and high performance Si anodes for the next generation Li-ion batteries in the near future.

Keywords: Lithium-ion battery; Nanomaterials; Anode; Silicon

* Corresponding author: lshaw2@iit.edu

Table of Contents

I. Introduction

Li ion batteries (LIBs) have revolutionized portable electronic devices in the past two decades, and have the potential to make great impact on vehicle electrification.[1] In spite of their eminent potential, the state-of-the-art Li-ion batteries (such as $LiCoO_2$/graphite batteries) have not been able to meet the need for vehicle electrification, requiring both high energy density and high power density with a long cycle life simultaneously.[2] Therefore, batteries with high energy density, high power density and long cycle life are in urgent demands to address the driving distance problem faced by LIBs. In this context, silicon is one of the most promising anode candidates for next-generation Li-ion batteries. This is due to its low voltage profile and high theoretical capacity (3590 mA h g^{-1} for $Li_{15}Si_4$ phase at room temperature),[3] which is about ten times that of carbonaceous materials including graphite, pyrolytic carbon and meso-phase pitch (about 372 mA h g^{-1}). In addition, silicon is the second ample element in the earth's crust. Therefore, mass production of silicon with low cost is not an issue. However, practical application of silicon anodes is currently hindered by multiple challenges including the enormous volume change (~ 300%) during lithiation/delithiation processes, low intrinsic electrical conductivity, and instability of the solid electrolyte interphase (SEI).[4, 5] The large volume change can result in particle pulverization, loss of electrical contact with the conductive additive or current collector, and even peeling off from the current collector. The repeated volume expansion and shrinkage also lead to fracture and re-formation of the SEI layer around the particles, resulting in continuous consumption of the electrolyte, increased impedance, and capacity fading.[4-10]

Significant efforts have been devoted to addressing the issues mentioned above. The strategies investigated include Si material design through nanostructures,[11-15] porous structures,[16-19] or nanocomposites,[20-22] Si electrode design with combined nano- and micro-particles [23] or with 3D micro-channels,[24] addition of electrolyte additives,[25] and use of novel binders.[26, 27] Thanks to the worldwide efforts, rapid advancements have been made in the properties and performance of Si anodes. These rapid advances have been reflected in a large number of review articles published recently.[2, 8-10, 28-39] In fact, just in 2014 alone there are 6 review articles on Si anodes,[8, 32-36] clearly indicating rapid expansion of research and advancements in the area of Si anodes. In spite of these outstanding reviews,[2, 8-10, 28-39] it is warranted that another review is due because significant advancements and breakthroughs have

been made in 2014 and 2015. Examples of such breakthroughs include exceptional specific and volumetric capacities at 1160 mA h g^{-1} and 1270 mA h cm^{-3}, respectively, after 1000 cycles at the C/2 rate accomplished through a pomegranate-inspired nanoscale design,[15] high specific and volumetric capacities at 1600 mA h g^{-1} and 1088 mA h cm^{-3}, respectively, after 150 cycles at 400 mA g^{-1} achieved via a micro-sized porous Si/C material,[18] and a specific capacity of 1450 and 1230 mA h g^{-1} after 100 cycles at 100 and 500 mA g^{-1}, respectively, obtained via a low cost, double-shelled Si@SiO_x@C core-shell structure.[40] However, none of these breakthroughs is included in 2014 reviews.[8, 32-35] Only one article published in 2014[41] is cited in these 2014 reviews. In contrast, in this review we have selected more than 25 articles[5, 13, 15, 18-22, 24, 40-55] published in 2014 and 2015 to highlight the new strategies and advancements made in the area of Si anodes. Furthermore, by integrating these 25+ articles with many previous publications we have provided a comprehensive overview on strategies in the Si material design, novel synthesis methods, and synthesis-structure-performance relationships to enhance the properties and performance of Si anodes, as outlined below.

In this review, we will start with an overview of the intrinsic properties of Si, followed by various strategies investigated so far to overcome the shortcomings of Si anodes. These strategies are grouped as follows: (i) particle-based structures (including nanoparticles, solid core-shell structure, hollow core-shell structure, and yolk-shell structure), (ii) porous Si designs, (iii) nanowires, nanotubes and nanofibers, (iv) Si-based composites, and (v) unusual designs. Finally, personal perspectives on outlook are offered with an aim to stimulate further discussion and ideas in the rational design of durable and high performance Si anodes for the next generation Li-ion batteries in the near future.

II. Intrinsic Properties of Silicon

Si has a theoretical capacity of 3590 mA h g^{-1} based on the fully alloyed form of $Li_{15}Si_4$ at room temperature,[3] and this value increases to 4200 mA h g^{-1} at high temperature corresponding to the formation of $Li_{22}Si_5$.[56] These capacities place Si on the top of all other anode materials except Li. As shown in Table 1,[57] Si has not only had the highest specific capacity, but also had the highest volumetric capacity among all the common anode materials investigated except pure Li metal.

Figure 1 shows the typical charge and discharge profiles of crystalline silicon.[3] The first lithiation (I region in Figure 1) leads to the formation of an amorphous phase. If the lithiation is continuous below 50 mV (II region), crystalline $Li_{15}Si_4$ will form. The subsequent delithiation (III region) results in amorphous Si which then becomes amorphous Li_xSi alloy in the following lithiation (IV region). Therefore, after the first charge/discharge cycle crystalline silicon has converted to amorphous and remains as amorphous in the further cycles.[3, 58] Figure 1 also shows that Si anodes can provide a very attractive working potential (~0.4 V vs. Li/Li^+), which is slightly higher than that of graphite anodes (~0.05 V vs. Li/Li^+) but can avoid the safety concern of lithium deposition upon cell overcharge.

The formation of the $Li_{15}Si_4$ phase leads to a large volume expansion (~300%).[3, 15, 34] The repeated volume expansion and shrinkage associated with lithiation and delithiation, respectively, can result in particle pulverization and loss of electrical contact with the conductive additive or current collector.[5-10] The repeated volume expansion and shrinkage also lead to fracture and re-formation of the SEI layer around the particles, resulting in continuous consumption of the electrolyte, increased impedance, and capacity fading.[4] It has been shown that volume expansion is anisotropic for crystalline Si,[48, 59] but becomes homogeneous for amorphous Si. Lithiation of crystalline Si is anisotropic too with the (110) surface more thermodynamically favorable for lithiation than (100) and (111) surfaces.[48, 60] In-situ TEM observations[61, 62] reveal that lithiation of crystalline Si particles occurs by movement of a two-phase boundary between the inner core of pristine Si and the outer shell of amorphous Li-Si alloy. In-situ TEM analysis of Si nanowires[63] and SEM observations of Si nanopillars[64] clearly show the anisotropic expansion of Si during lithiation. The anisotropic swelling of Si nanowires and nanopillars has been attributed to different interfacial energies of the amorphous Li-Si alloy and crystalline Si interface and thus different interface mobilities.[47, 63] It should be emphasized that these anisotropic lithiation and swelling behaviors are only applicable to the first lithiation cycle because after the first lithiation the initially crystalline Si remains amorphous in the subsequent cycling.[62]

In-situ TEM analysis has provided unambiguous evidence that large volume expansion during lithiation can result in cracking of Si particles.[61, 62] These in-situ TEM observations have revealed that there exists a critical particle diameter of ~150 nm below which Si particles will not crack.[61, 62] However, it is interesting to note that an early study suggests the critical size of Si

particles without cracking being < 20 nm.[11] Regardless of the precise number of the critical particle size, these studies do highlight the important role of nanostructure to yield high capacities.[65] Although nanoparticles do not crack, this feature alone is not sufficient because volume expansion and shrinkage still take place and can result in gradual loss of electrical contact with the conductive additive or current collector, leading to gradual capacity decay.[5, 40] As discussed below, nanostructures combined with other strategies often offer far better performance than nanoparticles alone.

A recent study[66] using mechanically clamped Si pillars to mimic the cluster of many crystalline Si particles in the confined volume within an anode shows that some beneficial effects of compressive stresses in suppressing crack formation during lithiation. Specifically, unclamped Si pillars have a critical diameter of ~300 nm above which cracking always occurs. However, when a <110> axially oriented Si pillar of 1 μm in diameter expands during lithiation with a gap of 300 nm to the walls (which oppose the expansion of Si when the Si pillar is in contact with them), only a few pillars exhibit noticeable cracking. When the diameter of the same Si pillar increases to 2.2 μm still with a gap of 300 nm to the walls, significant cracking occurs. These results are interesting and important because they provide evidence that the critical size of Si pillars for cracking can be increased from ~300 nm to larger than 1,000 nm. This phenomenon is expected to be applicable to Si particles with a mechanically robust, conductive coating. The latter can serve two purposes: offering highways for electron and Li-ion transport while suppressing the crack formation.

Silicon is a semiconductor and thus high purity Si has a very low electrical conductivity at room temperature (< 10^{-5} S cm^{-1}). However, doped Si (both n-type and p-type Si) can have electrical conductivities at ~10^{-2} S cm^{-1}.[67] These values are significantly lower than carbon and graphite which have electrical conductivity in the order of 10 to 10^{4} S cm^{-1},[68] but comparable with or higher than several oxide electrode materials such as $LiCoO_2$ (~10^{-4} S cm^{-1}), $LiMn_2O_4$ (~10^{-6} S cm^{-1}) and $LiFePO_4$ (10^{-9} S cm^{-1}).[68] Thus, conductive additives or coatings are necessary for fabrication of Si anodes.

III. Particle-Based Structures

Silicon in the particle morphology has been studied extensively. To facilitate discussion, we have classified Si particle-based structures in four categories (Figure 2). The first group is

nanoparticles including both solid and hollow particles (Figure 2a). The second group is solid core-shell structures in which Si serves as a core and the shell is typically an electronic and ionic conductor (Figure 2b). The third group is hollow core-shell structures in which the Si core is hollow (Figure 2c), whereas the conductive shell is the same as the solid core-shell structure. The last group is yolk-shell structures (Figure 2d), which have the void between the solid Si core and the outer conductive shell. These different particle structures respond to lithiation and delithiation differently, and thus have strong impact on the electrochemical performance of Si anodes, as described below.

3.1 Nanoparticles: Wang, et al. [40] has recently compared the cycling performance of micro-sized Si particles (1–2 μm) with those of nano-sized Si (~0.15 μm) with and without carbon coating. Their study clearly indicates that the nano-sized Si has a higher specific capacity and better capacity retention than that of the micro-sized Si, whereas the carbon-coated, nano-sized Si has the best performance (Figure 3). Specifically, the micro-sized Si possesses a specific capacity of 650 mA h g^{-1} after 100 cycles with a charge/discharge current of 100 mA g^{-1} and its capacity retention is only 20% when compared with the first charge capacity.[40] In contrast, the nano-sized Si exhibits a capacity of 1060 mA h g^{-1} after 100 cycles with its capacity retention at 38%, whereas the carbon-coated, nano-sized Si, a-Si@SiO_x/C (1/2.5), has the highest capacity (1450 mA h g^{-1}) and capacity retention (73%) after 100% cycles.[47] This set of data unambiguously reveals that capacity retention can be improved by reducing particle size because of the reduced tendency for particle cracking and smaller volume change per particle during cycles. The carbon coating can further improve the capacity retention probably because of the buffering effect of the coating. However, such a buffering effect may not be present in every system, as discovered in the other studies discussed below.

Pan, et al. [5] have carried out another comparison of commercial Si nanoparticles (~100 nm) with and without carbon coating, denoted as Si@C and Si, respectively, in Figure 4. The carbon coating is formed by carbonization of polydopamine (PODA). The formed Si@C particles are then etched with a NaOH aqueous solution to obtain a yolk-shell structure, Si@void@C, which is also included in Figure 4 for comparison. It can be seen that Si nanoparticles have the highest initial specific capacity, but their capacity decay very fast. With the carbon coating (5–8 nm thick) the capacity decay slows down, but eventually the capacity of Si@C approaches that of Si nanoparticles after 50 cycles, indicating that the effect of the carbon

coating is limited. In contrast, the Si@void@C yolk-shell structure exhibits superior capacity retention and still possesses 804 mA h g^{-1} after 50 cycles. The void in the yolk-shell structure provides space to accommodate volume expansion and shrinkage during cycles, whereas the carbon shell offers a stable interface for stability of the SEI layer and particle contacts between themselves and with the conductive additive and current collector. Therefore, nanoparticles alone are not sufficient to have good capacity retention. Engineering the particle structure by introducing voids to accommodate volume expansion is a promising strategy to improve the capacity retention.

Another way to introduce void to the particle structure is to synthesize hollow Si particles, as demonstrated by Yao, et al. [69] The hollow Si particles are formed by a template approach using solid silica nanospheres (350 nm in diameter). The silica nanospheres are drop-casted on a stainless steel sheet and a thin layer of silicon is subsequently deposited on the nanospheres through chemical vapor deposition (CVD) of SiH_4 at 485 ºC. The thickness of this Si shell is about 10 nm. At the end, the silica core is removed by dilute HF solution, leading to Si hollow spheres. These Si hollow spheres are interconnected and offer an initial discharge capacity of 2725 mA h g^{-1} which survives 700 cycles with capacity loss of 8% in every 100 cycles (Figure 5). The capacity retention is far better than that of solid nanoparticles because the void space in hollow Si spheres can accommodate volume expansion during lithiation and thus minimize the chance of crack forming in particles as well as reducing volume expansion outwards. The latter is important because little or no volume expansion outwards can lead to a stable SEI layer and good contact between particles and conductive additives.[4]

The work carried out by Kim, et al. [11] reveal that nanoscale particles (< 20 nm) are needed to avoid particle cracking, but optimization of particle sizes is required to obtain high specific capacities and good capacity retention over cycles. As shown in Figure 6, 5-nm Si nanoparticles have lower specific capacities than 10-nm and 20-nm Si nanoparticles in the entire range of the 40 cycles investigated. Interestingly, the specific capacities of all nanoparticles degrade gradually over the 40 cycles. However, the capacity decay becomes extremely small when 10-nm Si nanoparticles are coated with a carbon shell via chemical vapor deposition of acetylene at 500 ºC, indicating that confining the expansion of Si nanoparticles with a strong and conductive shell can greatly enhance the cycle stability.

3.2 Solid core-shell structures: The research discussed in Section 3.1 have revealed that a solid Si core with a conductive shell could offer some advantages over bare Si particles without coating. However, the advantages are limited in some cases because huge volume expansion of the Si core during lithiation still leads to volume expansion of the entire core-shell particle. This trend has been corroborated by several other studies, as discussed below. In addition, it can be reasoned that the mechanical properties of the conductive shell could play a critical role in suppressing or minimizing the volume expansion of the Si core, thereby leading to a more stable interface between particles and minimizing the fracture and re-formation of the SEI layer. Furthermore, the size of the Si core is also an important factor in dictating the cyclic stability since a small Si core results in small volume expansion. Motivated by these several possible mechanisms, different solid core-shell structures have been synthesized and studied.

Hwa, et al. [70] have prepared a solid core-shell material with Si nanoparticles (< 100 nm) as the core and amorphous carbon as the shell, denoted as n-Si@C hereafter. The process starts with uniform coating of nano-sized Si particles with polyvinyl alcohol (PVA). The mixed powder is then centrifuged and dried at room temperature. The next step is calcination at 750 ºC in Ar atmosphere for 3 h. The carbon shell was amorphous with a thickness about 5-10 nm (Figure 7). To better evaluate the electrochemical performance of this solid core-shell nanomaterial, batteries with Si nanoparticles without coating (n-Si), micro-sized Si particles (4 μm) coated with carbon (Si@C), and nano-sized Si particles coated with PVA (n-Si@PVA) are also fabricated. The results reveal that n-Si@C with a solid core-shell structure does not deliver the highest initial capacity, but it has the best capacity retention during cycling among all the cells studied, leading to a specific capacity of 1800 mA h g^{-1} after 50 cycles (Figure 7). n-Si@PVA has the second best capacity retention and delivers 500 mA h g^{-1} capacity after 50 cycles, whereas n-Si and Si@C exhibit poor capacity retention with less than 200 mA h g^{-1} capacity after 50 cycles (Figure 7). The superior properties of n-Si@C is attributed to the combined effect of the nanosize of the Si core and the conductive carbon coating.[70] The latter provides electrical conductivity and the buffering effect against the volume change during cycles. In contrast, the PVA shell in n-Si@PVA is not a conductor even though it can provide the buffering effect against the volume change during cycles.[70] Si@C does not possess good cycle stability because of the large Si core (4 μm), leading to large volume change in spite of the presence of the carbon shell. n-Si also displays poor performance because of the lack of the

positive effects provided by the carbon coating mentioned above. These results are in good accordance with the work by Kim, et al. [11] discussed in Section 3.1, showing extremely small capacity decay over cycles when 10-nm Si nanoparticles are coated with a carbon shell which provides the synergistic effects of the nano-Si core and enhanced electrical conductivity.

Another study on the solid core-shell structure is executed by Zhang, et al. [71] The polyacrylonitrile (PAN)-coated Si precursor is formed through the emulsion polymerization of acrylonitrile in the presence of Si nanoparticles. In the next step, the precursor is heated up to 800ºC and turned into a Si@C core-shell structure. The presence of the amorphous conductive carbon shell which covers the whole Si particles prevents combination of particles during charge/discharge cycles. To prove the enhanced performance of this core-shell structure, another anode from virginal Si nanoparticles is fabricated and tested. The capacity of the bare Si nanoparticles has faded quickly after a few cycles (20 cycles), but the Si@C core-shell structure can retain half of its initial capacity after the same number of cycles. This proves the enhanced cycling behavior of the core-shell structure.

The same research group has published another research paper on the synthesis and properties of Si@SiO core-shell structure synthesized through sol-gel reaction combined with the heating step.[72] Si nanoparticles (~50 nm) are coated with a solution of tetraethylorthosilicate (TEOS), ethanol and water at pH between 8 and 9. Then, aging process is done at 60 ºC for 1 h. The formed gel is dried at ambient temperature for 2 days followed by heating at 70 ºC for 6 h. After this step, all of the volatile compounds are completely removed from the material. The product is then ground to get fine powder and heated to 500 ºC for 6 h in an Ar atmosphere. The charge/discharge curves for this material indicates higher coulombic efficiency (CE) in the first cycle than pristine Si. As shown in Figure 8, after 20 cycles the reversible capacity is around 600 mA h g^{-1} which is better than the nano-sized Si anode (< 200 mA h g^{-1}). This can be attributed to the presence of the SiO shell which can result in half volume expansion (lithium silicates are formed) as compared to alloying between Si and Li ions. As a result, the SiO shell could act as a buffer and delay the collapse of the whole structure.

A double-walled core-shell structure has also been investigated. In this case, Si nanoparticles (100–200 nm) are coated with double shells, SiO_2 and C, and the material is denoted as Si@SiO_2@C.[43] Such a double-walled core-shell structure is synthesized by heating Si nanoparticles at 700 ºC for 2 h to from a silica layer around the particles, followed by

carbonization of epoxy resin at 700 ºC to form the outer carbon coating. Half-cells of this Si@SiO_2@C have been cycled between 0.01 and 5 V. Comparing to Si nanoparticles and carbon-coated Si nanoparticles (Si@C), this double-walled core-shell structure shows much better capacity retention (Figure 9). After 100 cycles the double-walled core-shell structure still exhibits a reversible capacity of 785 mA h g^{-1}, which is far better than the single core-shell structure (Si@C) investigated in the same study (Figure 9) as well as single core-shell structures Si@SiO[72] and Si@C[71] studied earlier by other groups (see, for example, Figures 7 and 8). The proposed electrochemical reaction for this double-walled core-shell structure is when Li ions diffuses in to the SiO_2 shell, they react irreversibly and form Li_4SiO_4 alloy (Equation 1). When Li ions reach the core silicon, reversible lithiation reaction occurs (Equation 2). This reaction determines the reversible capacity of the double-walled core-shell structure. This study[43] unequivocally shows that the properties of the shell are critical in improving the capacity retention of the Si anode. The thin interlayer SiO_2 enhances the adhesion of the carbon shell to the Si core and also alleviates stresses during cycles by acting as a buffering phase.

$$SiO_2 + 4Li^+ + 4e^- \rightarrow Li_4SiO_4 + Si \qquad \text{Equation 1}$$

$$Si + xLi^+ + xe^- \leftrightarrow Li_xSi \qquad \text{Equation 2}$$

Solid core-shell structures with the shell made of metals have also been investigated. Cetinkaya, et al. [44] have employed electroless deposition technique to prepare silicon/copper composite. First, silicon particles (~200 nm) are sensitized with $SnCl_2$ and then activated with $PdCl_2$. This pre-treatment makes the particle surface ready for deposition step. The deposition is done in a plating bath containing the copper sulfate precursor. The plating process is performed at room temperature and the coating around the silicon particles is uniform.[44] The mesoporous nature of copper layer facilitates the diffusion of Li ions along with the enhanced conductivity of silicon particles. The cycle stability of Cu-coated Si is better than that of bare Si, but the gradual decay in the capacity of Cu-coated Si leads to only a marginal enhancement in the specific capacity over bare Si (Figure 10), indicating that the Cu shell formed in this study is not very effective in improving the cycle stability of Si anodes.

Another study on Cu-coated Si is conducted by forming a Cu shell on submicrometer-sized Si particles (380, 620, 730 and 940 nm) through the polyol-mediated reduction of Cu (II) acetate in a Schlenk line under inert atmosphere.[73] The details of synthesizing submicrometer-sized Si particles are reported in Refs.[74, 75] Metallic Cu with a small portion of Cu_2O are

deposited around Si particles. The formation of copper oxide is due to trace water impurities in the solution or exposure of the powder to air after synthesis. The Cu-coated Si (380 nm particles) exhibit a stable capacity at ~600 mA h g^{-1} over 50 cycles,[73] which is much better than that obtained by Cetinkaya, et al. (Figure 10).[44] These results indicates that the quality of the Cu coating affected by synthesis conditions is important in determining the enhanced performance of Si anodes.

Solid core-shell structures with the shell made of TiO_2 have also been explored.[55] The TiO_2 coating is formed via sol-gel processing of TiO_2 in the presence of Si nanoparticles (70–100 nm). A specific capacity of 593 mA h g^{-1} is obtained after 50 cycles at 0.1C. This value is comparable with those obtained from Si@SiO,[72] n-Si@PVA,[70] and Si@Cu,[73] but much lower than those derived from double-walled Si@SiO_2@C,[43] n-Si@C with the Si core at 10 nm,[11] and n-Si@C with the Si core < 100 nm.[70] In another experiment, Tang, et al. [76] have devised a method to synthesize n-Si@TiN to address the volume change, pulverization, SEI layer accumulation, and conductivity problems of silicon anodes. First, TiO_2 coating is formed around Si nanoparticles by hydrolysis of titanium tetrabutoxide (TBOT). Then, the powder is annealed under N_2 atmosphere to convert TiO_2 to TiN. A comparson between n-Si and n-Si@TiO_2 reveals that the electrochemical performance of n-Si@TiN is much better, delivering 2,650 mA h g^{-1} at first discharge along with retaining 75% of initial capacity after 100 cycles.

Taking all of the aforementioned results together, one can conclude that a conductive shell on the surface of Si particles can improve the cycle stability. However, to achieve this desired effect, the following three factors need to be taken into account simultaneously. These are (i) the size of the Si core (less than 100 nm is a must), (ii) the material of the shell (being conductive and electrochemically stable), and (iii) synthesis conditions that lead to a uniform, mechanically strong, and conductive shell).

3.3 Hollow core-shell structures: Every limited studies have been conducted on hollow core-shell structures (Figure 2c) because hollow core-shell structures are far more difficult to synthesize than solid core-shell structures. One study conducted by Chen, et al. [77] does reveal that such a hollow core-shell structure can deliver outstanding performance. The hollow porous Si particles coated with the Ag shell, HPSi@Ag, are synthesized via a two-step synthesis (Figure 11a). Sol-gel SiO_2 is coated on the surface of polystyrene (PS) nanoparticles first, followed by calcination at 600 ºC to burn out the PS core and forma hollow porous silica ($HPSiO_2$) structure.

The latter is then subject to magnesiothermic reduction to obtain hollow porous silicon (HPSi) nanoparticles. The HPSi nanoparticles (about 200 nm) are then coated with a carbon shell (HPSi@C) or silver shell (HPSi@Ag) to form the hollow core-shell structures. Figure 11 summarizes some of the electrochemical testing results from the hollow core-shell structures. The charge and discharge capacities of the first cycle are 3146 and 3762 mA h g^{-1} with the coulombic efficiency of 84% for HPSi@Ag. The capacity remains high (~3000 mA h g^{-1}) after 100 cycles (Figure 11c). This is because of the synergistic combination of the nanostructured material and formation of the adequate void inside for volume expansion as well as the enhanced conductivity. In comparison, HPSi@C exhibits the second best performance, whereas HPSi nanoparticles show better performance than commercial solid Si nanoparticles. HPSi nanoparticles are doing better than solid Si nanoparticles because of the void inside to accommodate the volume expansion during lithiation. It is also worth mentioning that HPSi@Ag shows better results than HPSi@C, thanks to the higher electrical conductivity of Ag than that of carbon. HPSi@Ag nanoparticles also have excellent rate performance (Figure 11d). Moreover, the Ag coating has resulted in decreased charge transfer resistance as shown in the impedance plot (Figure 11e). Based on the electrochemical data, this structure can be a potential candidate for Si-based anodes in the next-generation Li-ion batteries.

3.4 Yolk-shell structures: Similar to solid core-shell structures, yolk-shell structures (Figure 2d) have been studied extensively[12, 13, 42, 45, 46, 78, 79] because they are relatively easier to synthesize than hollow core-shell structures. With yolk-shell structures the volume expansion of the Si particle inside the shell can be accommodated by the engineered void, whereas the conductive shell will allow electron and Li ion transport and offer a stable interface for good contact between various particles and the stability of the SEI layer. Multiple synthesis methods have been devised to form yolk-shell structures and thus different electrochemical properties are obtained.

Zhou, et al. [78] have synthesized the Si@void@C yolk-shell structure by coating silicon nanoparticles with a SiO_2 shell via sol-gel method, followed by coating the Si@SiO_2particles with carbon using sucrose at 800 ºC. Hydrofluoric acid (HF) is then used to dissolve the silica around the Si core, leading to the formation of the Si@void@C yolk-shell structure. The void between the core and shell provides sufficient space for expansion of the silicon core during lithiation without cracking in the carbon shell. Thermogravimetric analysis (TGA) reveals that

the weight percentage of silicon is about 28.54%. The yolk-shell electrode could deliver 813.9 mA h g^{-1} at the first cycle and retain ~500 mA h g^{-1} after 40 cycles (Figure 12). The Si@void@C material has a higher cyclability than Si nanoparticles and hollow carbon. The voltage profile reveals that intercalation of Li ions into the carbon shell and SEI layer formation occur between 0.1 and 0.9 V with an even slope, while incorporation of Li ions into silicon is shown with a long plateau in the potential curve.

Using a similar method, Tao, et al. [42] have also synthesized the Si@void@C yolk-shell structure, and obtained a very stable Si-based anode with ~780 mA h g^{-1} after 100 cycles. Further, they have examined the effect of carbon loading in the Si@void@C yolk-shell structure, and found that 63% carbon loading leads to a higher specific capacity (~780 mA h g^{-1}) than 72% carbon loading does (~690 mA h g^{-1}). This result indicates that optimization in the design of the Si@void@C yolk-shell structure is needed to maximize the specific capacity of yolk-shell structures.

Li, et al. [79] have used a slightly different approach to synthesize the Si@void@C yolk-shell structure. The starting material is 50 nm Si powder. After calcination at 600 ºC in the air, $SiO_2$is formed on the surface of the Si nanoparticles. The Si@SiO_2 particles are then coated with a thin layer of carbon (about 5 nm) inside a vacuum furnace. The next step is HF etching to remove all the traces of SiO_2 from the powder to form the Si@void@C yolk-shell structure. The electrode constructed from this yolk-shell structure displays a discharge capacity of 1400 and 1100 mA h g^{-1} in the first and second cycles, respectively. Afterwards the capacity decay becomes small, and ~750 mA h g^{-1} is retained after 60 cycles. This result is similar to those obtained by Zhou, et al. [78] and Tao, et al. [42] who have used a slightly different method to prepare the Si@void@C yolk-shell structure. In all of these studies,[42, 78, 79] the cycle stability of the Si@void@C yolk-shell structure is always better than those of Si nanoparticles and solid Si@C core-shell structures, unambiguously demonstrating the advantage of the engineered void in providing a space for the Si core to expand with no crack formation in the carbon shell.

An outstanding work in yolk-shell structures is conducted by Liu, et al. [12], who have fabricated this nanostructure from the commercial silicon nanoparticles. A SiO_2 sacrificial layer is coated on the surface of Si nanoparticles, followed by carbonization of a uniform layer of polydopamine to form the Si@SiO_2@C structure. Finally, HF etching through the porous carbon shell is carried out to remove SiO_2 and form the Si@void@C yolk-shell structure. The Si content

in Si@void@C is ~71 wt.% based on the TGA measurement.[12] The carbon shell formed in this study is very uniform, better than that reported by Li, et al.[79] As a result, outstanding cycle stability and high specific capacity are achieved. The capacity attained at 1C rate is ~1400 mA h g^{-1} after 1000 cycles, retaining 74% of the initial capacity with coulombic efficiency at 99.84% (Figure 13). In situ TEM has been employed to observe the lithiation/delithiation processes, in which Li ions penetrate to carbon shell and form alloy with silicon core. This study clearly reveals that well-engineered yolk-shell structures have the potential to serve as anodes for the next-generation LIBs.

Recently, yolk-shell structures with the shell made of SiO_2 have also been studied. Sun, et al. [45] have synthesized such a Si@void@SiO_2yolk-shell structure using a vesicle template method. It starts with the preparation of spherical micelles consisting of required surfactants. The addition of Si nanoparticles (about 30 nm diameter) along with a vesicle inducing agent into the micelle solution leads to the formation of Si-vesicle complex. Subsequent addition of SiO_2 precursor, TEOS, results in the formation of a vesicle–silica composite with a discrete silica layer in the palisade layer of the vesicles. After removing the surfactants by HCl, the Si@void@SiO_2 yolk-shell structure is formed. The SiO_2 shell formed in this study is mesoporous with channels to facilitate the lithium ion passage. It is found that the specific capacity of the Si@void@SiO_2 yolk-shell structure decreases with increasing the thickness of the SiO_2 shell from 10 nm to 40 nm. A large irreversible capacity is observed in the first cycle process, which is mostly due to the formation of a SEI layer on the surface SiO_2 shell and the irreversible electrochemical reactions between lithium ions and SiO_2 to form Li_2SiO_3 and Li_4SiO_4. After the first cycle, cycling performances are significantly improved due to the formation of a stable SEI layer on the silica shell surface. The reversible capacity can be retained at 687 mA h g^{-1} at a current density of 50 mA g^{-1} after 30 cycles.[45] This performance is slightly below that obtained from Si@void@C yolk-shell structures[42, 78, 79] and far below the well-synthesized Si@void@C yolk-shell structure,[12] suggesting that carbon is a better choice than SiO_2 for the shell material, presumably due to the better electrical conductivity of carbon than that of SiO_2.

Sun, et al.[46] have recently extended their vesicle template method[45] to form silicon/double-shelled carbon (Si@DC) yolk-like nanostructure (Figure 14). Their synthesis starts with the Si@void@SiO_2 yolk-shell structure made using the vesicle template method. The

Si@void@SiO_2 template is then coated with a glucose-derived polysaccharide on both interior and exterior surfaces of the porous SiO_2 shell. A subsequent annealing process at 800 ºC for 4 h under argon atmosphere results in the carbonization of the polysaccharide component, leading to the formation of a Si@void@C@SiO_2@C structure. Finally, the SiO_2 shell is dissolved in hydrofluoric acid to generate the Si@DC powders with a Si@void@C@void@C configuration. This dual yolk-shell material has a very high conductivity because of the presence of two carbon shells. The authors have also synthesized Si/single-shelled (Si@SC) and Si/three-shelled (Si@TC) nanopowders, but the best result is gained with Si@DC. As shown in Figure 14, the specific discharge capacity of Si@DC remains as high as 943.8 mA h g^{-1} at 50 mA g^{-1} after 80 cycles, which is higher than the Si@SC (719.8 mA h g^{-1}) and bare Si electrode (115.3 mA h g^{-1}).

The dual yolk-shell concept has also be explored with carbon and SiO_2 as the dual shells lately.[13] The dual yolk-shell structure in this case can be described as Si@void@SiO_2@void@C. To form this structure, Si nanoparticles are coated with a SiO_2 layer via the Stöber method and then the Si@SiO_2 particles are coated with a carbon layer. Taking advantage of the inhomogeneous nature of the silica shell prepared by the Stöber method, proper etching via HF treatment can selectively etch a small portion of the outer layer and a large portion of the interior layer of the SiO_2 shell, leading to the formation of the Si@void@SiO_2@void@C structure. In this dual yolk-shell structure, carbon improves the conductivity, while silica increases the mechanical stability and the void provides enough space for the volume expansion of the silicon core. Further, the SiO_2 and C dual shells can offer a double barrier to prevent the electrolyte from reaching the surface of the silicon nanoparticles and protect the anode from subsequent irreversible reaction with the electrolyte. The dual yolk-shell structure has exhibited superior capacity retention (83%) with a specific capacity at 956 mA h g^{-1} at a current density of 460 mA g^{-1} after 430 cycles, while the capacity of the Si@C core-shell structures decreases rapidly in the first ten cycles under the same experimental conditions (< 200 mA h g^{-1} after 430 cycles). The performance of this Si@void@SiO_2@void@C structure is much better than that of the Si@void@C@void@C structure,[46] indicating that the processing methods and conditions are important in realizing the potential of the dual yolk-shell design.

IV. Porous Silicon Designs

The principles using porous Si designs to enhance the performance of Si anodes are similar to those of hollow core-shell structures and yolk-shell structures, i.e., the void space introduced during synthesis can allow the silicon in the engineered structure to expand during lithiation with little or no change in the volume of the entire particle. This minimized volume expansion and shrinkage prevents particle fracture and leads to a stable SEI layer on the surface of the particle, while keeping all or most of particles in contact with conductive pathways. Multiple methods have been investigated to create various porous Si structures.[16-19, 80] Like hollow core-shell structures and yolk-shell structures, all of the porous Si designs studied so far have offered better electrochemical performance than bare Si nanoparticles or solid core-shell structures.[16-19, 80]

4.1 Nanosized porous silicon: Liu, et al. [17] have developed a novel method to produce mesoporous Si nanoparticles from the husks of rice, the second copious crop in the world. The method contains acid wash of rice husks, filtration, deionized water wash and calcination of the leached product at 700 ºC to yield nano-SiO_2. Magnesiothermic reduction of the nano-SiO_2 powder followed by acid etching is required to attain Si nanoparticles which have particle sizes ranging from 10 to 40 nm. BET measurement reveals the mesoporous nature of the collected particles (surface area of 245 m^2/g and pore volume of 0.74 cm^3/g). The mesoporous Si nanoparticles are utilized to make half-cells without any carbon coating. The results are extraordinary. The first cycle discharge capacity is 2790 mA h g^{-1}which reduces in the following cycles, but remains to be ~1700 mA h g^{-1} after 300 cycles at the C/2 rate. The capacity is ~2200 mA h g^{-1} after 100 cycles at the C/5 rate. The superior capacity and rate capability are attributed to nanoparticle sizes, large surface area, and the presence of mesopores to accommodate the volume expansion of Si during lithiation. The propensity of cracking and instability of SEI layers is further reduced by nanoparticle sizes, while large surface area shortens the diffusion path for Li ions enhancing the rate capability.[31]

4.2 Micro-sized porous silicon: Yi, et al. [16] have developed a different method to synthesize porous Si materials using nano-sized silicon particles as building blocks for micro-sized porous Si particles. The starting material is commercial micro-sized SiO powder which becomes Si/SiO_2 mixture after disproportionation at 950 ºC for 5 h (Figure 15). Subsequent HF etching of the Si/SiO_2 mixture results in the formation of micro-sized porous Si particles. Finally,

carbon coating of the porous Si is done by thermal decomposition of acetylene at 620 ºC for 20 min. SEM analysis reveals that the porous Si-C composite has an average particle size of 20 μm, while TEM analysis indicates that the interconnected Si nanoparticles which form the micro-sized particles have a size about 10 nm. Further, carbon is uniformly distributed among the interconnected Si nanoparticles. This porous Si-C material shows a higher capacity than bare silicon and could deliver 1459 mA h g^{-1} after 200 cycles at 1 A g^{-1} (Figure 15). In addition, it shows perfect rate performance of 700 mA h g^{-1} at 12.8 A/g. Further, its tap density is high (0.78 g/cm^3) and thus can give a high volumetric capacity (1326 mA h cm^{-3} at 400 mA g^{-1} after 50 cycles). The reported synthesis method is low cost and easy to scale up with a potential of mass production for the next-generation Li-ion batteries.

The same group has further examined the effect of disproportionation temperature on the size of Si nanoscale building blocks and found that Si building block sizes are 10, 15, 30 and 80 nm when the disproportionation temperature is 950, 1100, 1300 and 1400 ºC, respectively.[80] The initial charge/discharge capacities are found to increase with the disproportionation temperature because finer Si building blocks have larger surface areas and thus more surface SiO_2 present in the micro-sized porous Si/C materials (Figure 16). However, finer Si building blocks (10 and 15 nm) show far better cycling stability than larger Si building blocks (30 and 80 nm) because smaller building blocks have smaller volume change and thus more stable SEI layers. As shown in Figure 16, the micro-sized porous Si/C material with the Si building block at 15 nm has the best combination of these characteristics and thus exhibits the highest capacity at 1800 mA h g^{-1} (calculated based on the weight of Si and C in the porous material) after 100 cycles at a current density of 400 mA g^{-1}. The authors have also found out that carbon coating temperature at 800 ºC is better than 650 ºC because of the synergistic effect of better carbon quality (higher degree of graphitization and thus better electrical conductivity) and reduction of SiO_x on the surface of Si building blocks. The micro-sized porous Si/C material with carbon loading of ~20 wt.% deposited at 800 ºC exhibits a fixed capacity of 1200 mA h g^{-1} over 600 cycles at 1.2 A g^{-1} with a coulombic efficiency of 99.5% and no capacity decay.[80] As far as we know, this is the best cycling performance with such a high capacity for micro-sized Si-based anodes.

In another study,[19] micro-sized porous Al-Si particles are synthesized via a facile selective etching process of Al-Si alloy powder. Subsequent thin Al_2O_3 layers are introduced on the surface of the micro-sized porous Si particles via a selective thermal wet oxidation process of

the etched Al-Si particles. The resulting porous Si particles wrapped with thin Al_2O_3 layers offer outstanding cycling stability (a capacity retention of 78% of its original capacity of ~1000 mA h g^{-1} after 300 cycles at the C/5 rate) and excellent rate capability.

Other studies[18, 81-85] on micro-sized porous Si/C materials have also demonstrated high specific capacity with good cycling stability. Another important advantage of these micro-sized porous Si-based materials is their high tap densities. As a result, these porous materials also possess high volumetric capacity. For example, a recent study[18] reports a high volumetric capacity at 1088 mA h cm^{-3}, which is 5 times higher than that of commercially available nano-Si based anodes. Therefore, micro-sized porous Si-based materials are a strong contender as a high rate, high capacity, and cycling-stable anode for the next-generation LIBs.

V. Nanowires, Nanotubes and Nanofibers

One-dimensional (1D) nanowires, nanotubes and nanofibers have the advantage of allowing the expansion of silicon radially to minimize the cracking propensity. Furthermore, if an electrically conductive coating is present on the surface, these 1D nanowires, nanotubes and nanofibers can have robust electrical transport along the wire and tube axis while Li ion transport can be accomplished radially with a very short distance. As a result, these 1D nanowires, nanotubes and nanofibers can have high specific capacity and superior rate capability with long cycle stability.[4, 86-90] Indeed, one of the best electrochemical performances among all the Si anodes is achieved with double-walled silicon nanotubes [89]. However, one of the drawbacks for nanowires and nanotubes is that their electrode making process is different from the current powder-based electrode making process used commercially. New electrode making processes at low cost need to be developed for these emerging materials. Below are the key properties of Si nanowires and nanotubes obtained by various groups.

5.1 Silicon nanowires (SiNWs): Chan, et al. [4] have fabricated very small size nanowires which provide enough space for the expansion of silicon radially (Figure 17). These nanowires are made via chemical vapor deposition (CVD) of silicon on the stainless steel foil with stout mechanical and electrical properties.[4] Interestingly, these Si nanowires have the sufficient electronic conductivity along the longitudinal axis and can operate without the presence of any carbon. Figures 17a and 17b illuminate the differences between SiNWs and silicon particles by comparing the morphological changes before and after cycling. Exclusive electrochemical

performance of SiNWs are displayed in Figure 17c to 17d. Oxidation/reduction peaks of silicon can be observed in cyclic voltammogram (CV). The discharge capacity at first cycle is 3124 mA h g^{-1} and the battery could keep the capacity after 10 cycles with slight fading which is a sign of stable morphology and no loss of active materials. SiNWs can retain their capacity after 10 cycles which make them a potential candidate for replacing graphite which is currently used in regular Li-ion batteries.[14]

In the search for the facile and low cost synthesis method of SiNWs, Zhang, et al. [90] have introduced a novel crystalline silicon core with amorphous silicon oxide shell nanowires. In their process, silica and titanium powder as catalyst are mixed together and heated in the argon atmosphere up to 1,600 ºC. After characterization, the growth of SiNWs in the [111] direction is observed, but the growth mechanism is different from typical VLS growth. The authors have found that the formation of silicon spheres at lower temperatures (e.g. 1,400 ºC) facilitates the continuous growth of nanowires. The electrochemical performance of this material is fair, about 1,640 mA h g^{-1} discharge capacity after 100 cycles at 1 A g^{-1} current density.

5.2 Silicon nanowalls (SiNWLs): Wan, et al. [47] have designed and fabricated 2-dimensional Si nanowalls (SiNWLs) to address the large irreversible capacity loss during the first cycle. Since the 2-D nanowall structure design could reduce 50% of the specific surface area compared to the nanowire structure with similar geometric dimension, the SiNWLs will have less material exposed to the electrolyte. Thus, the design could limit the side reactions occurring at the anode-electrolyte interface which consume lithium ions to form SEI layers, and has improved the first coulombic efficiency to 83.4%. To fabricate the SiNWLs, nanoimprint lithography (NIL) method with deep reactive ion etching (DRIE) are utilized to create the periodic and disconnected nanowalls (Figure 18). Finite element package ABAQUS is used to simulate the mechanical deformation in the material. The results reveal the mean stress level's varying with time, and the distribution of the tensile mean stress at the mid-plane and outer surface is non-uniform. While the interior surfaces are more susceptible to form pores during the lithiation process triggered by the higher tensile mean stress in the middle part, the outer surfaces experience the pore formation in the delithiation process. As a result, the entire structure experiences a relatively homogeneous pore distribution after many cycles.

5.3 Silicon nanotubes (SiNTs): Silicon nanotubes (SiNTs) have attracted extensive attention. Park, et al. [87] have utilized Si nanotubes with a thin layer of carbon as a coating and by

this method, they allow Li ions to react on both the inner and outer surfaces of the tubes (Figure 19). The coin cells are fabricated with SiNTs and tested. At 0.2C rate, 3648 and 3247 mA h g^{-1} capacities are obtained in the first discharge and charge cycle, respectively. These capacities show a coulombic efficiency of 89% which is really high for the first cycle. The thin carbon layer is the main mechanism for this value of efficiency. The capacity at different charge and discharge rates show a stable and specific capacity of ~2700 mA h g^{-1} even after 200 cycles (Figure 19).

To achieve a method for large-scale production of SiNTs, Wen, et al. [88] have employed magnesiothermic reduction to convert silica nanotubes to SiNTs. First, silica nanotubes are synthesized with rod-like NiN_2H_4 as templating agent and TEOS as silica precursor. Next, silica powder is collected and reduced to SiNTs with magnesium powder at 660 ºC for 3 h in argon atmosphere. Etching with 0.5 M HCl removes unwanted products such as Mg_2Si and MgO. Rate capability and cycling performance of SiNTs are much better than Si particles (mesh 325). SiNTs have exhibited more than 1,000 mA h g^{-1} at 0.5C after 90 cycles while the Si particles could only deliver 500 mA h g^{-1}. The nanostructure helps to buffer the volume change of Si and also provides high surface area (113 m^2 g^{-1}) for lithium ion intercalation.

5.4 Double-walled silicon nanotubes (DWSiNTs): Wu, et al. [89] have developed double-walled silicon nanotubes (DWSiNTs) which combine two astonishing aspects together: the outer surface of this structure gives enough space for the stabilized growth of SEI layer and the inner space provides space for expansion of silicon during cycling. The internal structure contains Si while the external is made from SiO_x. Li ions can pass through the outer SiO_x layer and meanwhile this layer is strong enough to keep the structure integrity. The SEI layer forms around the outer tube uniformly, and this material has passed 6000 cycles at 12C without significant capacity loss (88% capacity retention). Figure 20 demonstrates some of the excellent electrochemical characteristics of this material. To our knowledge, 6000 cycles are the longest cycle life ever reported for Si anodes in the open literature.

5.5 Silicon nanofibers: In one of the recent studies, Hwang, et al. [91] have fabricated peculiar electrospun core-shell Si fibers. In their process the dual nozzle electrospinning machine is loaded with both the core polymer (containing Si nanoparticles and polymethylmethacrylate (PMMA) dissolved in N,N-dimethylformamide (DMF) and acetone) and the shell polymer (polyacrylonitrile (PAN) dissolved in DMF). One-dimensional fibers are formed in one step.

Subsequently, fibers are carbonized to convert PAN to the carbon shell and eliminate PMMA inside the Si core (Figure 21). Half-cells are made with these Si@C core-shell fibers and on each anode around 0.6 mg cm^{-2} of active material is loaded. A wide range of current densities is applied to the coin cell batteries fabricated with this material (from C/10 to 12C). At the lowest current density (C/10), the delivered capacities are reported as 1491 and 1305 mA h g^{-1} in the delithiation/lithiation procedure, respectively. This capacity is maintained quite well after 40 cycles. Further, at high current density (12C) the cells can still deliver a specific capacity of ~750 mA h g^{-1} (Figure 21), indicating high rate capability and good cycle stability.

Wu, et al. [92] have developed a slightly different method to synthesize Si@C core-shell nanofibers. In this process a SiO_2 precursor solution is mixed with Si nanoparticles first. With the aid of an electrospinning machine, Si/SiO_2 nanofibers are then generated from the suspension. To form the carbon coating, polystyrene as the carbon precursor is carbonized. The carbon layer is very thin and does not destroy the porous nature of the Si/SiO_2 core. The final step is etching with a HF solution to remove SiO_2. The entire method is low coast and scalable. Furthermore, the Si@C core-shell nanofibers are able to retain 90% of its original capacity and provide a specific capacity of ~870 mA h g^{-1} after 200 cycles, demonstrating the advantage of encapsulating silicon nanoparticles in carbon nanofibers.

An interesting modification of Si nanofibers is PPy@Si nanofibers fabricated by Du, et al.[93] The polypyrrole (PPy) fibers are produced by electropolymerization of pyrrole monomer, followed by uniform coating of Si on the fibers via CVD technique. The PPy core is inactive and acts as a backbone to provide the mechanical properties and enhance the electrical conductivity of nanofibers. This material is used as active material for the anode without any binder or conducting agent. The battery is tested for 100 cycles and it delivers more than 2800 mA h g^{-1}. These outstanding properties have been attributed to the conductivity and porous three dimensional network of the nanofibers which is perfect for volume expansion of silicon during cycling.[93]

Recently, Lee, et al. [94] have published a paper on fabrication of Si core/C shell nanofibers. This work is carried out by electrospinning machine equipped with a co-axial nozzle with two concentric cylinders. They have used PAN (polyacrylonitrile) as the carbonizing precursor, SAN (styrene-co-acrylonitrile) as the sacrificial core, and Si nanoparticles are loaded inside as the permanent core. The electrospun material is heated to burn the sacrificial core. The

obtained nanofibers are tested with contact lithiation. The results indicate no reaction between carbon and silicon and both the core and shell are lithiated separately. The silicon core volume expansion is confined completely inside the stable carbon shell. Initial charge capacity is reported as high as 967 mA h g^{-1} at 0.5 A g^{-1} current density with 92% capacity retention after 50 cycles.

VI. Si-Based Composites

Generally speaking, when Si is mixed with other materials, it is a Si-based composite. In this broad sense, almost everything that has been reviewed from Section III to Section V is a composite. To avoid confusion and repetition, however, we exclude everything that has been reviewed in Section III to Section V from the composite category, and focus our attention to three groups of Si-based composites. These are categorized as (i) Si/graphene and Si/nanographite sheet composites, (ii) Si/CNT, Si/CNF, and Si/graphite powder composites, and (iii) Si mixed with other material composites.

6.1 Si/graphene and Si/nanographite sheet composites: These composites have been studied extensively[51-54, 95] because graphene have outstanding electronic conductivity and can also serve as a substrate to constrain volume expansion of Si particles during cycles. Nanographite sheets can be considered as multi-layer graphenes, but with lower costs and lower electronic conductivities. The studies in this area have revealed that the addition of graphene can improve capacities and cycle stability, but graphene alone does not provide the best properties. The best electrochemical performance is obtained from the synergistic functions of graphene, carbon coating, and nano-sized Si, as discussed below.

Su, et al. [54] have developed a procedure to synthesize a Si/graphite@graphene composite with the structure of a Si/graphite mixture wrapped by graphene sheets. This composite is produced by mixing graphene oxide with nano-Si (30 nm) and graphite (~500 nm) in an alcohol solution, followed by spray-drying and then heating at 450^{o}C to reduce graphene oxide to graphene. The composite exhibits an initial charge capacity of 803 mA h g^{-1} at 100 mA g^{-1} and retain ~500 mA h g^{-1} after 50 cycles. The capacity decay slope, however, is close to a linear function of the cycle number, suggesting that the capacity retention needs to be improved in the future.

In a separate study carried out by Ma, et al. [52] carbon-coated Si nanoparticles supported by exfoliated graphite (EG) are synthesized by dispersing polyvinyl chloride (PVC)-coated Si nanoparticles (< 100 nm) with EG in a tetrahydrofuran (THF) solution, followed by heating the dried mixture at 900 ºC for 2 h in Ar atmosphere to convert PVC to carbon. The composite displays a high capacity of ~900 mA h g^{-1} at a current density of 200 mA g^{-1} and remains at this capacity over 40 cycles, indicating an excellent cycling stability. In contrast, carbon-coated Si nanoparticles only have a capacity of ~100 mA h g^{-1} at the same testing conditions after 40 cycles, unambiguously indicating the importance of EG as a flexible and conductive support in enhancing the cycling stability. In comparison with the study by Su, et al.,[54] this work also shows that carbon coating on Si nanoparticles is important for cycling stability even with the support of graphene or exfoliated graphite.

The synergistic effects of the carbon coating and graphene support in Si/graphene composites are further demonstrated by the work conducted by Yi, et al.[95] In their process micro-sized SiO and graphene oxide (GO) are first mixed in water with the presence of poly(diallydimethylammonium chloride) (PDDA) which serves as a positively charged medium to attract GO and SiO. The GO/PDDA-SiO mixture is then heated to 950 ºC for 5 h, followed HF etching at room temperature to create micro-sized porous Si supported by graphene (G/Si). Carbon coating is subsequently deposited on the surface of G/Si via thermal decomposition of acetylene at 800 ºC for 10 min. The carbon-coated, graphene-supported, micro-sized porous Si (denoted as G/Si-C) exhibits a high specific capacity (~1150 mA h g^{-1}) and remains at this level after 100 cycles (Figure 22). The outstanding capacity retention is attributed to the synergistic effects of the carbon coating, graphene support and porous Si with nano-sized building blocks. This well-engineered Si structure also allows high active material loading in the anode, leading to high areal capacities (3.2 mA h cm^{-2} after 100 cycles) with no decrease in the specific capacity (Figure 22b). In contrast, the specific capacity of the carbon-coated, micro-sized porous Si (Si-C) decreases sharply by high mass loading (Figure 22d), indicating the importance of the conductive function of graphene in linking all Si particles together regardless of their distance from current collector.

6.2 Si/CNT, Si/CNF, and Si/graphite powder composites: Carbon nanotubes (CNTs), carbon nanofibers (CNFs) and fine graphite particles can all provide electron transport pathways and serve as effective substrates to constrain volume expansion of Si particles during cycles.[50, 96,

[97] CNTs and CNFs have additional advantages over fine graphite particles in terms of their continuous electronic pathways, and thus are more effective in enhancing the electrochemical performance of Si anodes than fine graphite particles but at higher costs.

Zhang, et al. [50] have developed an interesting synthesis procedure to produce a low-cost Si/CNT&CNF composite made of carbon-coated Si nanoparticles interweaved with CNTs and CNFs, denoted as Si@C/CNTs&CNFs. Their synthesis procedure starts with ball milling of Si to form Si nanoparticles which are then mixed with citric acid in a nickel acetate-ethanol solution. The resulting suspension is then spray dried in N_2 atmosphere, followed by heating at 380 ºC for 4 h under N_2 atmosphere. These steps lead to Si@C particles with nickel oxide dispersed on their surfaces. The obtained Si@C particles are then subjected to a C_2H_2/N_2 treatment at 700 ºC for 3 h to form the Si@C/CNTs&CNFs composite. In this last step the nickel oxide acts as a catalytic agent to promote the growth of CNTs and CNFs. The obtained composite displays high capacities with superior cycling stability (1195 mA h g^{-1} after 50 cycles at 300 mA g^{-1}). By contrast, Si@C without CNTs and CNFs shows insufficient capacity retention (only 601 mA h g^{-1} after 50 cycles), whereas Si nanoparticles without carbon coating have the worst performance with its capacity dropping to nearly zero after 15 cycles.[50] The performance of Si@C better than Si nanoparticles is in good accordance with a large number of studies discussed in Sections 3.1 and 3.2. The best performance of Si@C/CNTs&CNFs has been attributed to the function of CNTs and CNFs in providing continuous electronic pathways by linking most of Si@C particles together and offering the void space (interweaved with Si@C particles) to absorb the volume expansion in lithiation, thereby great reduction in the conduction network breakage during cycles and thus superior cycling stability.[50]

In a separate study,[97] the importance of linking most of Si nanoparticles together by a conductive network has also been demonstrated. In this study Si nanoparticles are attached to graphite microparticles which provide a conductive network to allow fast charge and discharge of Si nanoparticles with superior cycle stability. A polymer blend consisting of poly(diallyl dimethyl-ammonium chloride) and poly(sodium 4-styrenesulfonate) is used to enable uniform distribution of Si nanoparticles on graphite microparticles and serve as a robust artificial solid-electrolyte interphase. Due to these synergistic effects, the composite electrode displays a specific capacity of 450 mA h g^{-1}, 96% capacity retention at a 10C rate, and 95% retention after 200 cycles.[97]

6.3 Si mixed with other material composites: This group can include Si/ceramic, Si/polymer, Si/metal, and Si/intermetallic composites. This group can offer positive surprises if the design principles to solve the Si anode problems are followed.[20-22, 24, 98] Several examples along this direction are presented below.

An interesting example of Si/ceramic/metal/carbon composites is the a-Si-SiO_x/Cr/C composite made lately by Li, et al. [20] A simple, scalable two-step method is used to synthesize such a composite. The commercial SiO powder is first subjected to disproportionation reaction at 1000 ºC for 3 h to form the Si/SiO_x nanoscale mixture which is then ball milled with micro-sized Cr and graphite powders. As shown in Figure 23, the obtained composite exhibits a high specific capacity (810 mA h g^{-1}) with capacity retention close to 100% over 200 cycles at a current density of 100 mA/g. For comparison, other composites without graphite (a-Si-SiO_x/Cr), without Cr (m-c-Si-SiO_x/graphite), and without Cr and graphite (m-c-Si-SiO_x) have synthesized and tested. All of them have displayed poor cycling stability (Figure 23). It is found that the high hardness of Cr powder has resulted in the formation of a-Si-SiO_x in very fine particle sizes during ball milling. As a result, small volume change takes place per particle during cycles, thereby minimizing the loss of particle contact and the stress causing the fracture and re-formation of SEI layers.[20] It should be emphasized that the specific capacity reported in this study is based on the total weight of the a-Si-SiO_x/Cr/C composite. Combining its high capacity and outstanding capacity retention with its low cost and easily scalable processing method, this composite has the potential to serve as anodes for LIBs in the future.

Han, et al. [22] have also utilized high-energy ball milling to synthesize a Si/silicide nanocomposite. The synthesis consists of two straightforward steps with the first step being arc melting of an elemental mixture of Si, Fe and Cr to create a $Si_{80}Fe_{16}Cr_4$ master alloy and the second being high-energy ball milling of the master alloy for 8 or 10 h to create the uniformly mixed Si + $FeSi_2$ + $CrSi_2$ nanocomposite. The composite can deliver an initial delithiation capacity ~900 mA h g^{-1} and remain at ~840 mA h g^{-1} at 1C rate after 100 cycles, showing an excellent capacity retention behavior.[22] The primary factors contributing to the excellent electrochemical performance are the size reduction of Si particles to nanometer scale (~5 nm), the formation of the highly elastic $FeSi_2$ + $CrSi_2$ matrix which can accommodate the volume change of Si, and separation of the silicide phases from Si after extended cycling.[22]

High-energy ball milling has also been studied to make Si/polymer composites. In one of the earliest studies,[98] a polypyrrole (PPy) film is ball milled with commercial Si to form the Si/PPy composite. Mixing silicon nanoparticles with PPy fulfils two requirements. First, PPy is a conductive polymer and thus improves the conductivity of the composite. Second, it also acts as buffer to prevent crack formation and pulverization of silicon. The composite is able to deliver 1800 mA h g^{-1} at the first discharge which, however, is suppressed to lower values at subsequent cycles, indicating that improvements are needed in order to compete with other Si anode technologies in the future.

High-energy ball milling typically leads to uniformly mixed composite structures, as shown above. To obtain particle structures other than uniformly mixed composites, different methods have to be devised. Lee, et al. [21] have explored electrical wire explosion of a Ni wire in a Si nanoparticle-dispersed suspension with oleic acid (OA) as the liquid medium to produce a Ni-Si nanocolloidal suspension. The Ni-Si colloids are then dried and subjected to a 500^{o}C heat treatment to carbonize OA and form carbon-coated Ni-Si nanocomposites. The resultant composite is composed of the Ni (5 to 10 nm) and Si (~100 nm) particle mixture coated with a thin carbon layer (~5 nm). The Ni-Si@C nanocomposites are able to deliver high reversible capacities of ~3500 and 2000 mA h g^{-1} of Si at current densities of 84 and 840 mA/g of Si, respectively, whereas the bare Si nanoparticle electrode examined under the same conditions only possesses specific capacities of ~1200 and 280 mA h g^{-1} of Si, respectively. The outstanding electrochemical performance of the Ni-Si@C nanocomposite has been attributed to i) the distributed small Ni nanoparticles and carbon coating improve the surface electrical conductivity of the Si nanoparticles, resulting in a highly efficient conducting network of the electrode; ii) the uniform carbon coating surrounding each Ni-Si particle effectively buffers the stress of volume excursions and acts as a barrier against the reaggregation of the nanoparticles during repeated cycles; and iii) the high pore volume and large specific surface area of the nanocomposite facilitate the rapid penetration of the electrolyte and provide a large contact area between the electrolyte and the electroactive surface of the Ni-Si@C nanocomposites, thereby providing efficient transport of Li ions throughout the electrode and a high specific capacity, as well as sufficient void space to absorb the volume expansion.

VII. Unusual Designs

Some of the Si material designs have unique features and do not fall into any categories discussed above. Thus, we have assigned them to the "unusual designs" category. Because of their unique structures these unusual designs often possess exceptional properties. Here we have selected several of them to highlight their synthesis strategies and structure-property relationships.

7.1 Hollow porous silica nanocubes (HPSNCs): Yan, et al. [99] have developed a two-step hard-templating process to fabricate silica nanocubes. $Co_3[Co(CN)_6]_2$ nanoparticles are employed as the primary core and coated with silica using tetraethyl orthosilicate (TEOS) as the precursor (Figure 24). After annealing at 550ºC, the $Co_3[Co(CN)_6]_2$ core becomes Co_3O_4 which is then etched away by hydrochloric acid to acquire hollow porous silica nanocubes. At the first cycle, HPSNCs are able to deliver 3,048 and 1,457 mA h g^{-1} for discharge and charge, respectively, with the coulombic efficiency of 47% (Figure 24). The huge difference between the first discharge and charge is due to the formation of SEI layer around the particles and the reaction of silica with Li ions. After the second cycle, the capacity fading is decelerated for the rest 28 cycles and a specific capacity of ~1,000 mA h g^{-1} is retained after 30 cycles. This performance makes these nanocubes a potential rival for nanospheres.

7.2 Pomegranate-inspired silicon nanoparticles: A pomegranate-inspired nanoscale design for the silicon anode is proposed by Liu, et al. [15] lately. In this pomegranate microbead structure, the Si particle structure is engineered at two-length scales. First, individual Si@C yolk-shell particles are formed with sizes ~100 nm. Second, these yolk-shell nanoparticles are clustered together to form secondary particles of sizes 1 to 10 μm (Figure 25). Such a pomegranate-inspired Si structure is synthesized through a series of processing steps including (i) coating commercial silicon nanoparticles with a SiO_2 layer using sol-gel process with TEOS as the precursor, (ii) self-assembling of Si@SiO_2 nanoparticles in a water-in-oil emulsion to form the assembled Si@SiO_2 clusters of 1 to 10 μm in diameter, iii) heat treatment at 550 ºC for 1 h in air to remove the organics and condense the cluster structures, iv) formation of a resorcinol-formaldehyde resin (RF) layer to wrap the Si@SiO_2 cluster, which is converted into a carbon layer under argon at 800 ºC, and v) finally, the SiO_2 sacrificial layer is removed with 5 wt.% HF solution to form the yolk-shell structure in each individual nanoparticles.

The advantages of this pomegranate-inspired microbead structure is that the electrolyte is blocked out of the cluster instead of forming SEI layers on each individual nanoparticles, while the void space in individual yolk-shell particles can accommodate the large volume change of silicon during the charge/discharge process. Therefore, this pomegranate-inspired design addresses three fundamental challenges faced by nanostructured electrodes simultaneously: a) high surface area (leading to significant SEI formation and low coulombic efficiency), b) low tap density (thus low volumetric capacity), and c) generally poor electrical properties due to the high interparticle resistance (resulting in poor cycle life). Indeed, the pomegranate microbead structure shows remarkable battery performance with a specific capacity of 2,350 and 1,160 mA h g^{-1} at C/20 and C/2 rates, respectively, after 1,000 cycles (Figure 25). Furthermore, this electrode has reached an areal capacity as high as 3.1 mA h cm^{-2} with a high solid loading of 3.12 mg cm^{-2} at the anode. To the best of our knowledge, there are only two engineered Si structures can reach an areal capacity above 3.0 mA h cm^{-2}. The other one is the carbon-coated, graphene-supported, micro-sized porous Si.[95] Both of these breakthroughs were accomplished in 2014.

7.3 Crab shell templates: To address the issues of high cost and complex synthesis process of nanostructures, Yao, et al. [100] have conceived the idea of using nature available crab shell fibers as bio-templates to synthesize Si electrodes. The highly mineralized chitin-protein fibers, when being removed during thermal calcination, leave a twisted plywood $CaCO_3$ template with nanoscale channels of ~70 nm in diameter. The $CaCO_3$ template is then coated with a uniform carbon layer, followed by depositing a Si layer inside the nano-channels via CVD. The $CaCO_3$ core is subsequently dissolved while the hollow carbon nanofiber arrays are remained to encapsulate the silicon nanotube (Figure 26). The battery made with this material shows a reversible specific capacity maintained at ~2,010 mA h g^{-1} after 200 cycles at C/2 rate. The superior properties have been ascribed to the combined effects of the hollow Si nanostructure and the robust outer carbon shell. The former provides sufficient space for the volume expansion of Si during cycles, while the latter reduces deleterious interactions of the active material with the electrolyte and forces the Si to expand inwards during cycling. The high electrochemical performance of this material and the huge availability of the natural precursors promise a bright future in the field of low cost nanomaterials synthesis.

7.4 Prelithiated Si anodes: Si nanostructures (e.g., nanoparticles, core-shell and yolk-shell nanostructures, nanowires, nanotubes, nanocomposites, etc.) can all offer improvements in cycle life over coarse Si particles. However, the drawback of these nanostructures is that their high surface area increases SEI formation in the first and later cycles. As a result, the first-cycle Coulombic efficiency of Si anodes is typically low in the range of 50% to 80%.[101] One method to improve the irreversible capacity loss in the first cycle is prelithiation. Zhao, et al. [101] have synthesized artificial SEI-protected Li_xSi nanoparticles via a two-step synthesis method. The prelithiation agent is able to prelithiate both alloying and intercalating type anode materials. First, the Li_xSi nanoparticles are prepared by mixing Si NPs and Li metal at 200 ºC for 3 days under mechanical stirring to form a crystalline Li_xSi core. Second, the crystalline Li_xSi core is coated with an amorphous inert layer by reduction of 1-fluorodecane. The process is similar to the SEI formation in battery and the coating thickness can be controlled by changing the oxidant concentration. Once the artificial SEI-coated Li_xSi NPs is in contact with the electrolyte, the Li_xSi NPs are reactivated and help improve the first cycle Coulombic efficiency to 99.2%, avoiding the huge first cycle capacity loss. These artificially SEI-coated NPs eliminates lithium consumption to form SEI layer around particles and helped to solve irreversible capacity decay problem.

Prelithiation also provides the possibility of coupling prelithiated Si anodes with cathodes containing no Li (such as S cathodes). Liu, et al. [86] have proposed a facile method based on self-discharge mechanism to prelithiate SiNWs. Nanowires are grown on a stainless steel substrate and a lithium foil is placed on the top of the SiNWs with the electrolyte added in between.[86] Under the highly spontaneous chemical reaction (driving force, ΔG = -42 kJ/mol), SiNWs are lithiated to 50% of their theoretical capacity within 20 minutes with little or no change in the morphology of SiNWs. The prelithiated SiNWs have been pared with a sulfur-based cathode to evaluate the effectiveness of prelithiation. The full cell can maintain ~80% of its initial capacity after 10 cycles, but it decays with a constant slope throughout cycling. The prelithiation on SiNWs enlightened the possibility of utilizing lithium-free materials as future lithium ion battery electrode. However, additional work is needed to optimize the performance of full cells.

Forney, et al. [102] have established a novel method to prelithiate silicon-carbon nanotube (Si/CNT) using stabilized lithium metal powder (SLMP). By prelithiating Si/CNT, the lithium introduced could compensate the lithium consumption during SEI formation process, and this

will lead to an increase in the capacity retention especially in the first cycle. The SLMP prelithiated Si/CNT is synthesized by SLMP deposition (drop-cast SLMP/toluene onto SI/CNT) followed by pressure activation and 40-50 h of equilibration. The pressure activation is crucial to ensure the contact and diffusion of lithium into the anode, and the equilibration helps SLMP to reach a stable state of prelithiation and achieve capacity matching between the anode and cathode. This treatment on Si/CNT anode has eliminated 20-40% of capacity loss in the first cycle, achieving >1,000 cycles at 20% depth of discharge.

VIII. Summary and outlook

Silicon has a higher theoretical capacity (3590 mA h g^{-1}) than other materials for Li-ion battery anodes. However, its practical application is impeded by three major challenges: large volume expansion during cycling (~300%), low electrical conductivity, and instability of the SEI layer caused by repeated volume change of the Si material. Enormous research efforts have been devoted to addressing these challenges. The strategies studied so far include reducing particle sizes to nanoscale, pursuing conductive coatings or conductive networks, providing void space during synthesis to accommodate volume expansion, introducing highly elastic phases to mitigate the deleterious effect of large volume change, and a combination of these strategies.

To compare the effectiveness of the different strategies investigated so far, Si material designs with the best performance obtained to date have been summarized in Table 2. The list in this table is selected based on two criteria. First, the cycle number demonstrated needs to be 100 or higher. Second, the specific capacity needs to be high (near 1000 mA h g^{-1}) or exceptionally long cycle life has been demonstrated (such as 6000 cycles). Several general trends can be extracted from this table. First, all of the designs, regardless of their morphology (particles, tubes, fibers, or films), use nanoscale Si as the building block to form Si anodes, demonstrating that reducing the building block to nanoscale is essential in minimizing the volume change per particle during cycles. Second, most of the Si material designs pursue conductive coatings or introducing conductive networks to improve the electrical conductivity of the Si anode and, in some cases, to confine Si volume expansion inside the conductive coatings. Third, many Si material designs with outstanding performance are associated with the introduction of void space during synthesis. In fact, only three material designs that have made into the list in Table 2 do not introduce void space during synthesis, and all of these designs (i.e., Si@SiO_x@C,

Si@SiO_2@C, and Si/silicide composite) have only been cycled up to 100 cycles. In contrast, several Si material designs with engineered void space have exhibited stable cyclability up to 1000 cycles or more with high specific capacities. Finally, the best performance of Si anodes with high specific capacity and long cycle life is attained through well-designed internal structures by combining multiple strategies including nanoscale building blocks, conductive coatings or networks, and engineered void space. The best examples of such Si material designs are pomegranate-inspired Si design[15] and carbon-coated, graphene-supported, micro-sized porous Si.[95] Both of these designs not only have high specific capacities with long life, but also possess high areal capacities (> 3.0 mA h cm^{-2}) at high mass loading. The latter is very important for high specific capacities at the cell level, and thus is essential for practical applications in LIBs.

The research conducted so far has identified many effective strategies to address the issues of Si anodes, and significant advancements have been made. With continuous innovations of Si anode designs on geometric structure and trials on different combinations of functional material composites, silicon's outstanding properties as an anode material could be exploited to the most. However, the search for finding the optimized internal structure for silicon to harvest its theoretical capacity has not ended yet. The continue advancements in the following several directions will be essential for the eventual broad market penetration of Si-based LIBs, and thus we anticipate that these areas will attract significant attention in the next several years.

1. Si anodes with high mass loading: Anodes with high Si mass loading and high areal capacities are essential for practical applications. Well-designed anodes such as pomegranate-inspired Si design[15] and carbon-coated, graphene-supported, micro-sized porous Si[95] have demonstrated the possibility of achieving such a goal. However, further improvement is desired. One of the approaches to further enhance Si mass loading while improving electrochemical performance is by increasing the tap density of Si anodes. During writing of this review, an article describing such an effort is published.[103] In this article, a new method that starts with mechanical pressing of silica-coated Si nanoparticles (Si@SiO_2) to produce high tap density silicon anodes is described. The mechanically pressed pellets are then subjected to thermal sintering at 600 ºC for 2 h to link nanoparticles together before ball milling to form micrometer-sized powder which is then coated with carbon to form Si@SiO_2@C particles of 1 to 15 μm in size. The last step is etching to remove silica and provide enough empty spaces for silicon

volume change. The tap density obtained through this approach is 0.91 g cm^{-3}, about doubles the value of pomegranate-inspired Si design.[15] The anode made using these micrometer-sized particles can have mass loading as high as 2.02 mg cm^{-3} with a high areal capacity of ~3.5 mA h cm^{-2} at current density of 0.1 mA cm^{-2}. The authors also demonstrate that with the addition of carbon nanotubes to the micrometer-sized particles the rate capability can be further enhanced.

2. Low cost synthesis and processing methods: Well-designed anodes such as pomegranate-inspired Si design[15] and carbon-coated, graphene-supported, micro-sized porous Si[95] have demonstrated the possibility of high specific capacities with long life as well as high areal capacities (> 3.0 mA h cm^{-2}) at high mass loading. However, synthesis methods for these well-engineered Si structures are often very elaborate and, in some cases, addition of expensive carbon nanotubes and graphene is sought. For widespread applications of high performance Si anodes the cost will eventually determine the fate of high performance Si anodes. For example, both carbon black and graphene can improve electrical conductivity, but the cost of graphene is more than 10,000 times that of carbon black. Therefore, we expect that low cost synthesis and processing methods which are scalable at industry setting will be an important area for research in the next several years. The latest article[103] has made a significant step towards this direction.

3. Prelithiated anodes: Research conducted so far[86, 101, 102] have clearly shown that prelithiation is an effective method to improve the irreversible capacity loss in the first cycle. Prelithiation also allows the formation of batteries by coupling of Li-Si alloy anodes with cathodes containing no Li. However, the first investigation of batteries made of a Li-Si alloy anode versus a sulfur cathode reveals that significant efforts are needed in the future to improve the cycle stability of such a battery.[86] Another area that deserves attention is the integration of prelithiated Si with conductive coatings. The latter will provide three functions simultaneously: (i) serving as a highway for electron and Li-ion transport, (ii) confining Si volume change within the conductive shell, and (iii) offering a stable interface for SEI formation and contact between particles during cycling. As the Si core has been prelithiated, the first reaction is delithiation along with volume shrinkage. This should reduce the propensity of Si cracking drastically.

4. Self-healing binders: Although this review focuses on Si anode design, it should be pointed out that the challenges faced by Si anodes should also be addressed by advancing other components such as electrolytes and binders. Lately, Wang, et al. [104] have shown that the cycling stability of silicon microparticles (SiMPs) can be improved drastically by utilizing a self-healing

polymer (SHP) binder. This polymer confines the SiMPs' large volume expansion and helps to keep the contact among broken Si particles, which ensures a stable cycling performance as well as high capacity retention. To improve conductivity and mechanical properties of SHP, carbon black nanoparticles are consolidated in the structure of polymer. This polymer shows superior properties comparing to polyvinylidene fluoride (PVDF), carboxymethyl cellulose (CMC) and alginate binders. The first cycle discharge capacity of 2,617 mA h g^{-1} at 0.4 A g^{-1} is achieved while 80% of this value is retained after 90 cycles. Recently, the same researchers have published another paper[105] reported high areal capacity anode (3-4 mA h cm^{-2}) with 3D distribution of SHP in the optimized Si matrix. After comparing silicon particles with different size distributions, the authors have concluded that selection of Si particle sizes and their distributions is important for full utilization of self-healing binders and Si particles with 500 nm – 1.5 μm size distribution (with 800 nm peak) are found to exhibit the best electrochemical performance.

5. Properties and behavior of Si in multiple cycles: In-situ TEM analysis[61-63] of the expansion and cracking behavior of Si pillars,[64, 66] and density functional theory (DFT) calculations[48, 60] have improved drastically our understanding of the intrinsic properties and behavior of Si under electrochemical loading. However, most of these studies have been focused on the first cycle lithiation. Thus, efforts in studying the intrinsic properties and behavior of Si under multiple cycles are urgently needed since all practical applications require many cycles. Fundamental understanding along this direction will provide guidelines for rational design of Si anodes that can pave the way for broad market penetration of Si-based LIBs.

In conclusion, we expect the design and synthesis of Si anodes to remain a very active area in the near future. By overcoming the volume expansion, low conductivity and unstable SEI problem of silicon, the best anode materials with extremely high capacity and huge availability will be ready for the revolution of the lithium ion battery field. We are optimistic to witness the breakthrough on Si anode applications and the future blooming of lithium ion batteries as the energy solution for future.

Acknowledgements – MA and LS are grateful to the Rowe Family Endowment Fund, and QH acknowledges Tang Fellowship.

References

1. J. M. Tarascon and M. Armand, *Nature*, 2001, **414**, 359-367.
2. D. Larcher, S. Beattie, M. Morcrette, K. Edstrom, J.-C. Jumas and J.-M. Tarascon, *Journal of Materials Chemistry*, 2007, **17**, 3759-3772.
3. M. Obrovac and L. Krause, *Journal of The Electrochemical Society*, 2007, **154**, A103-A108.
4. C. K. Chan, H. Peng, G. Liu, K. McIlwrath, X. F. Zhang, R. A. Huggins and Y. Cui, *Nature nanotechnology*, 2008, **3**, 31-35.
5. L. Pan, H. Wang, D. Gao, S. Chen, L. Tan and L. Li, *Chemical Communications*, 2014, **50**, 5878-5880.
6. S. D. Beattie, D. Larcher, M. Morcrette, B. Simon and J.-M. Tarascon, *Journal of The Electrochemical Society*, 2008, **155**, A158-A163.
7. M. Holzapfel, H. Buqa, L. J. Hardwick, M. Hahn, A. Würsig, W. Scheifele, P. Novák, R. Kötz, C. Veit and F.-M. Petrat, *Electrochimica acta*, 2006, **52**, 973-978.
8. B. Liang, Y. Liu and Y. Xu, *Journal of Power Sources*, 2014, **267**, 469-490.
9. H. K. Liu, Z. Guo, J. Wang and K. Konstantinov, *Journal of Materials Chemistry*, 2010, **20**, 10055-10057.
10. W.-J. Zhang, *Journal of Power Sources*, 2011, **196**, 13-24.
11. H. Kim, M. Seo, M.-H. Park and J. Cho, *Angewandte Chemie International Edition*, 2010, **49**, 2146-2149.
12. N. Liu, H. Wu, M. T. McDowell, Y. Yao, C. Wang and Y. Cui, *Nano letters*, 2012, **12**, 3315-3321.
13. L. Y. Yang, H. Z. Li, J. Liu, Z. Q. Sun, S. S. Tang and M. Lei, *Sci. Rep.*, 2015, **5**.
14. J. Graetz, C. Ahn, R. Yazami and B. Fultz, *Electrochemical and Solid-State Letters*, 2003, **6**, A194-A197.
15. N. Liu, Z. Lu, J. Zhao, M. T. McDowell, H.-W. Lee, W. Zhao and Y. Cui, *Nat Nano*, 2014, **9**, 187-192.
16. R. Yi, F. Dai, M. L. Gordin, S. Chen and D. Wang, *Advanced Energy Materials*, 2013, **3**, 295-300.
17. N. Liu, K. Huo, M. T. McDowell, J. Zhao and Y. Cui, *Sci. Rep.*, 2013, **3**.
18. J. Song, S. Chen, M. Zhou, T. Xu, D. Lv, M. L. Gordin, T. Long, M. Melnyk and D. Wang, *Journal of Materials Chemistry A*, 2014, **2**, 1257-1262.
19. G. Hwang, H. Park, T. Bok, S. Choi, S. Lee, I. Hwang, N.-S. Choi, K. Seo and S. Park, *Chemical Communications*, 2015, **51**, 4429-4432.
20. M. Li, J. Gu, X. Feng, H. He and C. Zeng, *Electrochimica Acta*, 2015, **164**, 163-170.
21. D.-H. Lee, H.-W. Shim and D.-W. Kim, *Electrochimica Acta*, 2014, **146**, 60-67.
22. H. K. Han, C. Loka, Y. M. Yang, J. H. Kim, S. W. Moon, J. S. Cho and K.-S. Lee, *Journal of Power Sources*, 2015, **281**, 293-300.
23. M. Wu, J. E. C. Sabisch, X. Song, A. M. Minor, V. S. Battaglia and G. Liu, *Nano Letters*, 2013, **13**, 5397-5402.
24. J. S. Kim, W. Pfleging, R. Kohler, H. J. Seifert, T. Y. Kim, D. Byun, H.-G. Jung, W. Choi and J. K. Lee, *Journal of Power Sources*, 2015, **279**, 13-20.
25. N.-S. Choi, K. H. Yew, K. Y. Lee, M. Sung, H. Kim and S.-S. Kim, *Journal of Power Sources*, 2006, **161**, 1254-1259.
26. A. Magasinski, B. Zdyrko, I. Kovalenko, B. Hertzberg, R. Burtovyy, C. F. Huebner, T. F. Fuller, I. Luzinov and G. Yushin, *ACS Applied Materials & Interfaces*, 2010, **2**, 3004-3010.
27. I. Kovalenko, B. Zdyrko, A. Magasinski, B. Hertzberg, Z. Milicev, R. Burtovyy, I. Luzinov and G. Yushin, *Science*, 2011, **334**, 75-79.
28. C. M. Hayner, X. Zhao and H. H. Kung, *Annual review of chemical and biomolecular engineering*, 2012, **3**, 445-471.
29. C.-M. Park, J.-H. Kim, H. Kim and H.-J. Sohn, *Chemical Society Reviews*, 2010, **39**, 3115-3141.

30. J. Wen, Y. Yu and C. Chen, *Materials Express*, 2012, **2**, 197-212.
31. M. Ge, X. Fang, J. Rong and C. Zhou, *Nanotechnology*, 2013, **24**, 422001.
32. D. Ma, Z. Cao and A. Hu, *Nano-Micro Letters*, 2014, **6**, 347-358.
33. N. Nitta and G. Yushin, *Particle & Particle Systems Characterization*, 2014, **31**, 317-336.
34. M. L. Terranova, S. Orlanducci, E. Tamburri, V. Guglielmotti and M. Rossi, *Journal of Power Sources*, 2014, **246**, 167-177.
35. X. Su, Q. Wu, J. Li, X. Xiao, A. Lott, W. Lu, B. W. Sheldon and J. Wu, *Advanced Energy Materials*, 2014, **4**, 1300882.
36. H. Kim, E.-J. Lee and Y.-K. Sun, *Materials Today*, 2014, **17**, 285-297.
37. Y. Yin, L. Wan and Y. Guo, *Chinese Science Bulletin*, 2012, **57**, 4104-4110.
38. R. Teki, M. K. Datta, R. Krishnan, T. C. Parker, T.-M. Lu, P. N. Kumta and N. Koratkar, *Small*, 2009, **5**, 2236-2242.
39. M. Gu, Y. He, J. Zheng and C. Wang, *Nano Energy*, 2015.
40. D. Wang, M. Gao, H. Pan, J. Wang and Y. Liu, *Journal of Power Sources*, 2014, **256**, 190-199.
41. P. Zhang, L. Wang, J. Xie, L. Su and C.-a. Ma, *Journal of Materials Chemistry A*, 2014, **2**, 3776-3782.
42. H. Tao, L.-Z. Fan, W.-L. Song, M. Wu, X. He and X. Qu, *Nanoscale*, 2014, **6**, 3138-3142.
43. H.-C. Tao, X.-L. Yang, L.-L. Zhang and S.-B. Ni, *Ionics*, 2014, **20**, 1547-1552.
44. T. Cetinkaya, M. Uysal, M. O. Guler, H. Akbulut and A. Alp, *Powder Technology*, 2014, **253**, 63-69.
45. Z. Sun, X. Song, P. Zhang and L. Gao, *RSC Advances*, 2014, **4**, 20814-20820.
46. Z. Sun, S. Tao, X. Song, P. Zhang and L. Gao, *Journal of The Electrochemical Society*, 2015, **162**, A1530-A1536.
47. J. Wan, A. F. Kaplan, J. Zheng, X. Han, Y. Chen, N. J. Weadock, N. Faenza, S. Lacey, T. Li, J. Guo and L. Hu, *Journal of Materials Chemistry A*, 2014, **2**, 6051-6057.
48. J. Rohrer, A. Moradabadi, K. Albe and P. Kaghazchi, *Journal of Power Sources*, 2015, **293**, 221-227.
49. D. Wang, M. Gao, H. Pan, Y. Liu, J. Wang, S. Li and H. Ge, *Journal of Alloys and Compounds*, 2014, **604**, 130-136.
50. M. Zhang, X. Hou, J. Wang, M. Li, S. Hu, Z. Shao and X. Liu, *Journal of Alloys and Compounds*, 2014, **588**, 206-211.
51. T. Mori, C.-J. Chen, T.-F. Hung, S. G. Mohamed, Y.-Q. Lin, H.-Z. Lin, J. C. Sung, S.-F. Hu and R.-S. Liu, *Electrochimica Acta*, 2015, **165**, 166-172.
52. C. Ma, C. Ma, J. Wang, H. Wang, J. Shi, Y. Song, Q. Guo and L. Liu, *Carbon*, 2014, **72**, 38-46.
53. Y. Zhang, Y. Jiang, Y. Li, B. Li, Z. Li and C. Niu, *Journal of Power Sources*, 2015, **281**, 425-431.
54. M. Su, Z. Wang, H. Guo, X. Li, S. Huang, W. Xiao and L. Gan, *Electrochimica Acta*, 2014, **116**, 230-236.
55. D. Yan, Y. Bai, C. Yu, X. Li and W. Zhang, *Journal of Alloys and Compounds*, 2014, **609**, 86-92.
56. R. A. Huggins, *Journal of Power Sources*, 1999, **81**, 13-19.
57. N. Liu, W. Li, M. Pasta and Y. Cui, *Front. Phys.*, 2014, **9**, 323-350.
58. P. Limthongkul, Y.-I. Jang, N. J. Dudney and Y.-M. Chiang, *Journal of Power Sources*, 2003, **119**, 604-609.
59. X. H. Liu, H. Zheng, L. Zhong, S. Huang, K. Karki, L. Q. Zhang, Y. Liu, A. Kushima, W. T. Liang and J. W. Wang, *Nano letters*, 2011, **11**, 3312-3318.
60. M. K. Y. Chan, C. Wolverton and J. P. Greeley, *Journal of the American Chemical Society*, 2012, **134**, 14362-14374.
61. X. H. Liu, L. Zhong, S. Huang, S. X. Mao, T. Zhu and J. Y. Huang, *ACS Nano*, 2012, **6**, 1522-1531.
62. M. T. McDowell, I. Ryu, S. W. Lee, C. Wang, W. D. Nix and Y. Cui, *Advanced Materials*, 2012, **24**, 6034-6041.

63. X. H. Liu, J. W. Wang, S. Huang, F. Fan, X. Huang, Y. Liu, S. Krylyuk, J. Yoo, S. A. Dayeh, A. V. Davydov, S. X. Mao, S. T. Picraux, S. Zhang, J. Li, T. Zhu and J. Y. Huang, *Nat Nano*, 2012, **7**, 749-756.
64. S. W. Lee, M. T. McDowell, L. A. Berla, W. D. Nix and Y. Cui, *Proceedings of the National Academy of Sciences*, 2012, **109**, 4080-4085.
65. M. Armand and J.-M. Tarascon, *Nature*, 2008, **451**, 652-657.
66. S. W. Lee, H.-W. Lee, I. Ryu, W. D. Nix, H. Gao and Y. Cui, *Nat Commun*, 2015, **6**.
67. M. Neuberger, *Silicon: Electrical Conductivity Data Sheets*, DTIC Document, 1963.
68. M. Park, X. Zhang, M. Chung, G. B. Less and A. M. Sastry, *Journal of Power Sources*, 2010, **195**, 7904-7929.
69. Y. Yao, M. T. McDowell, I. Ryu, H. Wu, N. Liu, L. Hu, W. D. Nix and Y. Cui, *Nano letters*, 2011, **11**, 2949-2954.
70. Y. Hwa, W.-S. Kim, S.-H. Hong and H.-J. Sohn, *Electrochimica Acta*, 2012, **71**, 201-205.
71. T. Zhang, L. Fu, J. Gao, L. Yang, Y. Wu and H. Wu, *Pure and applied chemistry*, 2006, **78**, 1889-1896.
72. T. Zhang, J. Gao, H. P. Zhang, L. C. Yang, Y. P. Wu and H. Q. Wu, *Electrochemistry Communications*, 2007, **9**, 886-890.
73. S. Murugesan, J. T. Harris, B. A. Korgel and K. J. Stevenson, *Chemistry of Materials*, 2012, **24**, 1306-1315.
74. J. T. Harris, J. L. Hueso and B. A. Korgel, *Chemistry of Materials*, 2010, **22**, 6378-6383.
75. L. E. Pell, A. D. Schricker, F. V. Mikulec and B. A. Korgel, *Langmuir*, 2004, **20**, 6546-6548.
76. D. Tang, R. Yi, M. L. Gordin, M. Melnyk, F. Dai, S. Chen, J. Song and D. Wang, *Journal of Materials Chemistry A*, 2014, **2**, 10375-10378.
77. D. Chen, X. Mei, G. Ji, M. Lu, J. Xie, J. Lu and J. Y. Lee, *Angewandte Chemie International Edition*, 2012, **51**, 2409-2413.
78. X.-y. Zhou, J.-j. Tang, J. Yang, J. Xie and L.-l. Ma, *Electrochimica Acta*, 2013, **87**, 663-668.
79. X. Li, P. Meduri, X. Chen, W. Qi, M. H. Engelhard, W. Xu, F. Ding, J. Xiao, W. Wang, C. Wang, J.-G. Zhang and J. Liu, *Journal of Materials Chemistry*, 2012, **22**, 11014-11017.
80. R. Yi, F. Dai, M. L. Gordin, H. Sohn and D. Wang, *Advanced Energy Materials*, 2013, **3**, 1507-1515.
81. H. Kim, B. Han, J. Choo and J. Cho, *Angewandte Chemie*, 2008, **120**, 10305-10308.
82. B. M. Bang, J.-I. Lee, H. Kim, J. Cho and S. Park, *Advanced Energy Materials*, 2012, **2**, 878-883.
83. B. M. Bang, H. Kim, H.-K. Song, J. Cho and S. Park, *Energy & Environmental Science*, 2011, **4**, 5013-5019.
84. A. Magasinski, P. Dixon, B. Hertzberg, A. Kvit, J. Ayala and G. Yushin, *Nat Mater*, 2010, **9**, 353-358.
85. J.-I. Lee, N.-S. Choi and S. Park, *Energy & Environmental Science*, 2012, **5**, 7878-7882.
86. N. Liu, L. Hu, M. T. McDowell, A. Jackson and Y. Cui, *ACS Nano*, 2011, **5**, 6487-6493.
87. M.-H. Park, M. G. Kim, J. Joo, K. Kim, J. Kim, S. Ahn, Y. Cui and J. Cho, *Nano Letters*, 2009, **9**, 3844-3847.
88. Z. Wen, G. Lu, S. Mao, H. Kim, S. Cui, K. Yu, X. Huang, P. T. Hurley, O. Mao and J. Chen, *Electrochemistry Communications*, 2013, **29**, 67-70.
89. H. Wu, G. Chan, J. W. Choi, I. Ryu, Y. Yao, M. T. McDowell, S. W. Lee, A. Jackson, Y. Yang, L. Hu and Y. Cui, *Nat Nano*, 2012, **7**, 310-315.
90. C. Zhang, L. Gu, N. Kaskhedikar, G. Cui and J. Maier, *ACS Applied Materials & Interfaces*, 2013, **5**, 12340-12345.
91. T. H. Hwang, Y. M. Lee, B.-S. Kong, J.-S. Seo and J. W. Choi, *Nano Letters*, 2011, **12**, 802-807.
92. H. Wu, G. Zheng, N. Liu, T. J. Carney, Y. Yang and Y. Cui, *Nano Letters*, 2012, **12**, 904-909.
93. Z. Du, S. Zhang, Y. Liu, J. Zhao, R. Lin and T. Jiang, *Journal of Materials Chemistry*, 2012, **22**, 11636-11641.

94. B.-S. Lee, S.-B. Son, K.-M. Park, J.-H. Seo, S.-H. Lee, I.-S. Choi, K.-H. Oh and W.-R. Yu, *Journal of Power Sources*, 2012, **206**, 267-273.
95. R. Yi, J. Zai, F. Dai, M. L. Gordin and D. Wang, *Nano Energy*, 2014, **6**, 211-218.
96. L. Shao, J. Shu, K. Wu, X. Lin, P. Li, M. Shui, D. Wang, N. Long and Y. Ren, *Journal of Electroanalytical Chemistry*, 2014, **727**, 8-12.
97. F.-S. Li, Y.-S. Wu, J. Chou and N.-L. Wu, *Chemical Communications*, 2015, **51**, 8429-8431.
98. Z. Guo, J. Wang, H. Liu and S. Dou, *Journal of Power Sources*, 2005, **146**, 448-451.
99. N. Yan, F. Wang, H. Zhong, Y. Li, Y. Wang, L. Hu and Q. Chen, *Sci. Rep.*, 2013, **3**.
100. H. Yao, G. Zheng, W. Li, M. T. McDowell, Z. Seh, N. Liu, Z. Lu and Y. Cui, *Nano Letters*, 2013, **13**, 3385-3390.
101. J. Zhao, Z. Lu, H. Wang, W. Liu, H.-W. Lee, K. Yan, D. Zhuo, D. Lin, N. Liu and Y. Cui, *Journal of the American Chemical Society*, 2015, **137**, 8372-8375.
102. M. W. Forney, M. J. Ganter, J. W. Staub, R. D. Ridgley and B. J. Landi, *Nano Letters*, 2013, **13**, 4158-4163.
103. D. Lin, Z. Lu, P.-C. Hsu, H. R. Lee, N. Liu, J. Zhao, H. Wang, C. Liu and Y. Cui, *Energy & Environmental Science*, 2015, **8**, 2371-2376.
104. C. Wang, H. Wu, Z. Chen, M. T. McDowell, Y. Cui and Z. Bao, *Nat Chem*, 2013, **5**, 1042-1048.
105. Z. Chen, C. Wang, J. Lopez, Z. Lu, Y. Cui and Z. Bao, *Advanced Energy Materials*, 2015, **5**, 1401826.

Tables and Figures

Table 1. Properties of some anode materials proposed for Li-ion batteries. Reproduced with permission[57] © 2014, Springer.

Materials	Li	C	$Li_4Ti_5O_{12}$	Si	Ge	Sn
Density (g cm^{-3})	0.53	2.25	3.5	2.3	5.3	7.3
Lithiated phase	Li	LiC_6	$Li_7Ti_5O_{12}$	$Li_{4.4}Si$	$Li_{4.4}Ge$	$Li_{4.4}Sn$
Density of lithiated phase (g cm^{-3})	0.53	2.20	3.65	1.18	2.04	2.56
ICDD PDF card number	(00-001-1131)	(00-034-1320)	(00-049-0207)	(01-077-2882)	(00-017-0402)	(00-018-0753)
Theoretical specific capacity in delithiated state (mA h g^{-1})	∞	372	175	4200	1620	993
Theoretical specific capacity in lithiated state (mA h g^{-1})	3860	339	168	2010	1140	790
Theoretical volumetric capacity in delithiated state (mA h cm^{-3})	∞	837	613	9660	8600	7250
Theoretical volumetric capacity in lithiated state (mA h cm^{-3})	2050	747	614	2370	2330	2020
Volume change (%)	∞	12	1	410	370	260
Potential versus Li/Li^+ (V)	0	0.05	1.6	0.4	0.5	0.6

Notes:
1. Theoretical volumetric capacity = Theoretical specific capacity × Density
2. Volume change (%) = (Volume of lithiated phase ÷ Volume of delithiated phase –1) × 100

Table 2. Some Si material designs with promising capacities and cycle stability.

Si material design	Specific capacity after cycling (mA h g^{-1})	Charge-discharge cycles demonstrated	Ref.
Si@SiO_x@C	1450	100	40
Si@SiO_2@C	785	100	43
Interconnected hollow Si spheres	1526	700	69
Hollow Si@Ag core-shell structure	3000	100	77
Si@void@C yolk-shell structure	1400	1000	12
Si@void@SiO_2@void@C double yolk-shell structure	956	430	13
Si@void@C yolk-shell structure	780	100	42
Nano-sized porous Si	2200	100	17
Carbon-coated, micro-sized porous Si	1459	200	16
Carbon-coated, micro-sized porous Si	1200	600	80
Carbon-coated Si nanotubes	2700	200	81
Double-walled Si nanotubes	590	6000	89
Carbon-coated, graphene-supported, micro-sized porous Si	1150*	100	95
Si/silicide composite	840	100	22
Pomegranate-inspired Si design	1160*	1000	15

* Only these two designs have achieved an areal capacity higher than 3.0 mA h cm^{-2}.

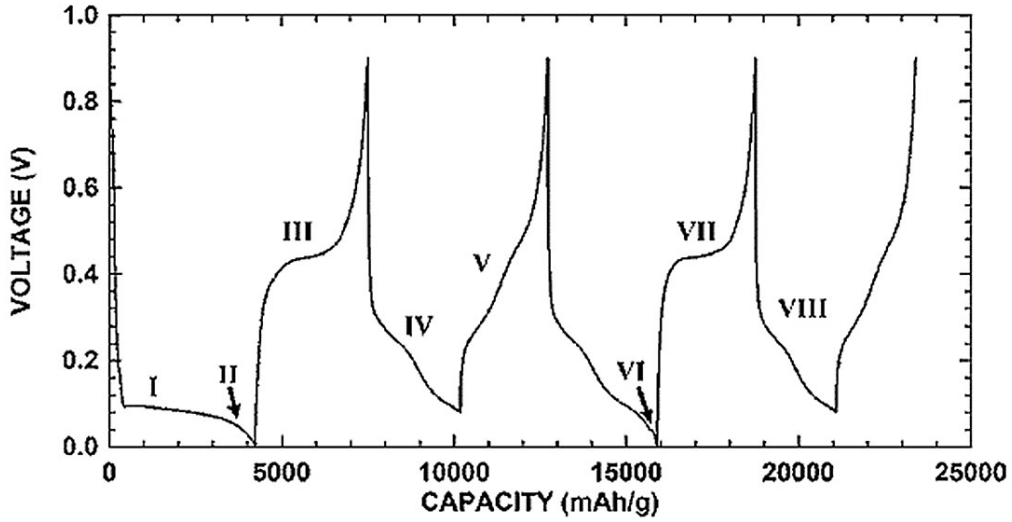

Figure 1. Charge/discharge voltage profile of micro-sized Si. Reproduced with permission[3] © 2007, The Electrochemical Society.

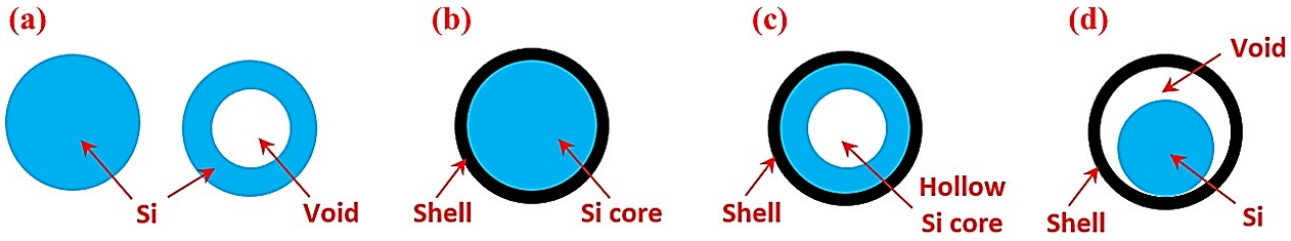

Figure 2. Si particles with different internal architectures: (a) solid and hollow particles, (b) solid core-shell structures, (c) hollow core-shell structures, and (d) yolk-shell structures.

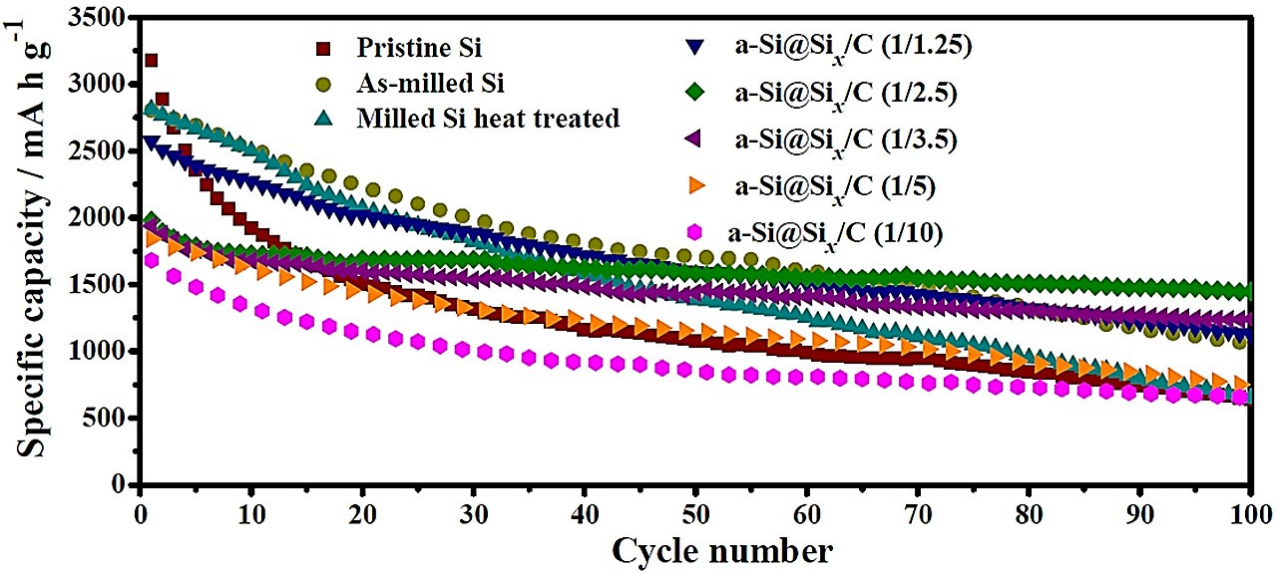

Figure 3. Cycling performance of amorphous Si@SiO_x/C core-shell particles in comparison with micro-sized Si particles (pristine Si) and nano-sized Si@SiO_x without carbon coating (as-milled Si). The SiO_x layer is due to the oxidation of Si particles in the ambient atmosphere and thus is ultrathin, whereas the carbon coating is formed via carbonization of citric acid. The number in the parenthesis after a-Si@SiO_x/C stands for the Si-to-citric acid ratio. Reproduced with permission[40] © 2014, Elsevier.

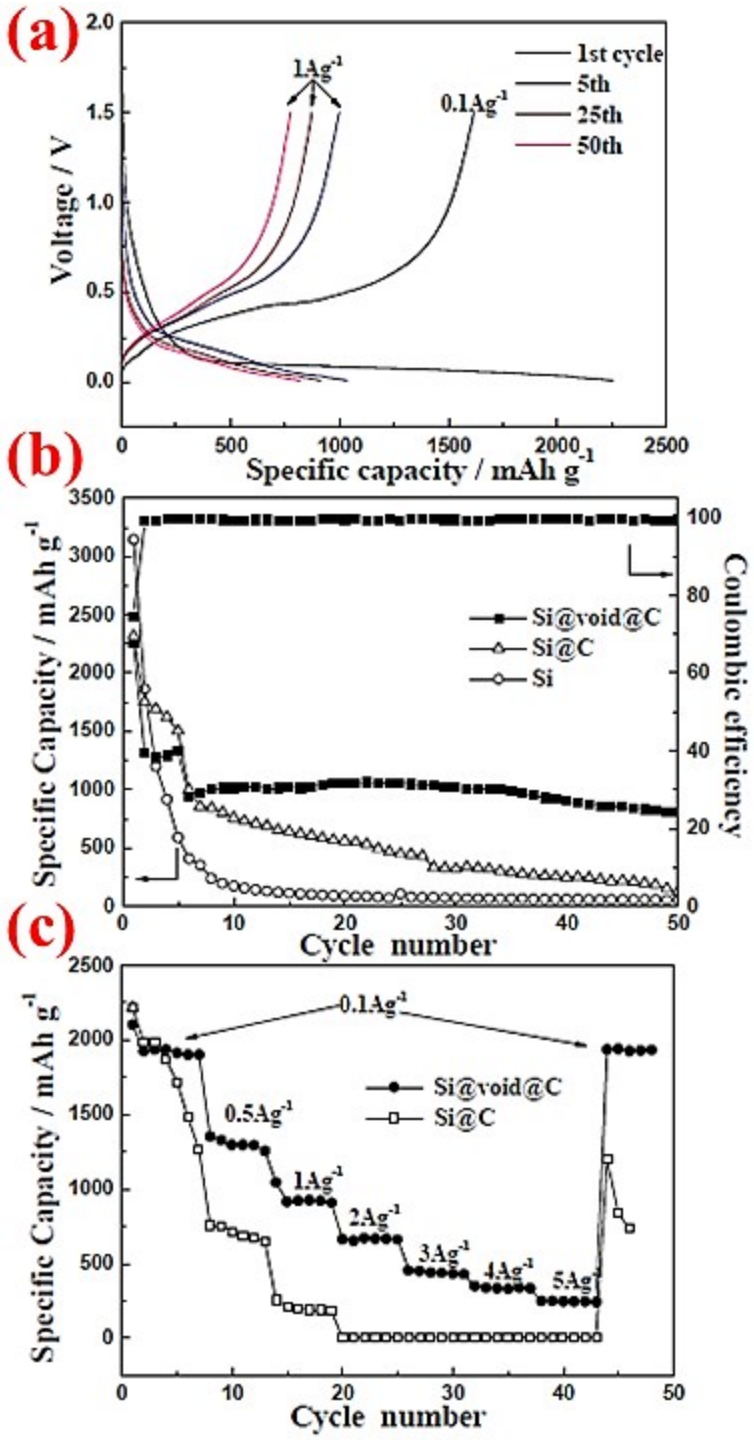

Figure 4. Electrochemical performance of commercial Si nanoparticles (~100 nm) with and without carbon coating, denoted as Si@C and Si, respectively, in comparison with that of a yolk-shell structure, Si@void@C. Reproduced with permission[5] © 2014, The Royal Society of Chemistry.

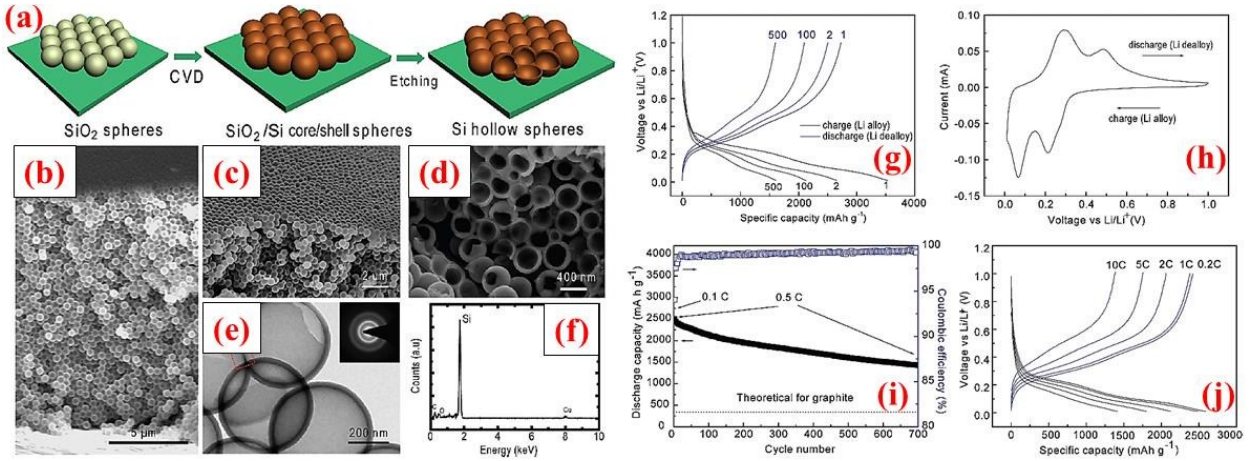

Figure 5. (a) Hollow silicon spheres formation process; (b-f) characterization data, and (g-j) electrochemical results. Reproduced with permission[69] © 2011, American Chemical Society.

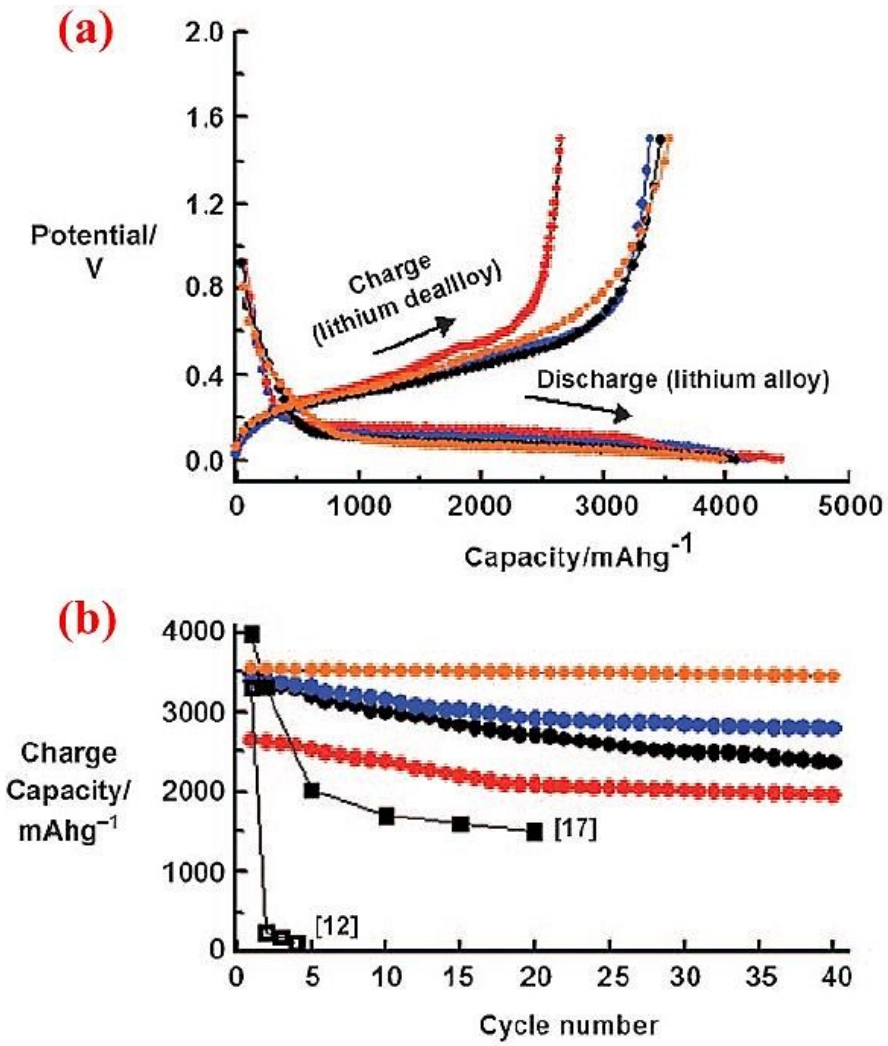

Figure 6. a) Voltage profiles of 5, 10, and 20 nm sized n-Si and 10 nm sized n-Si after carbon coating during the first cycle in coin-type half-cells at a rate of 0.2 C between 0 and 1.5 V. b) Plot of charge capacity versus cycle number (red: 5 nm, blue: 10 nm, orange: 10 nm after carbon coating, black circles: 20 nm). Reproduced with permission[11] © 2010, Wiley-VCH Verlag.

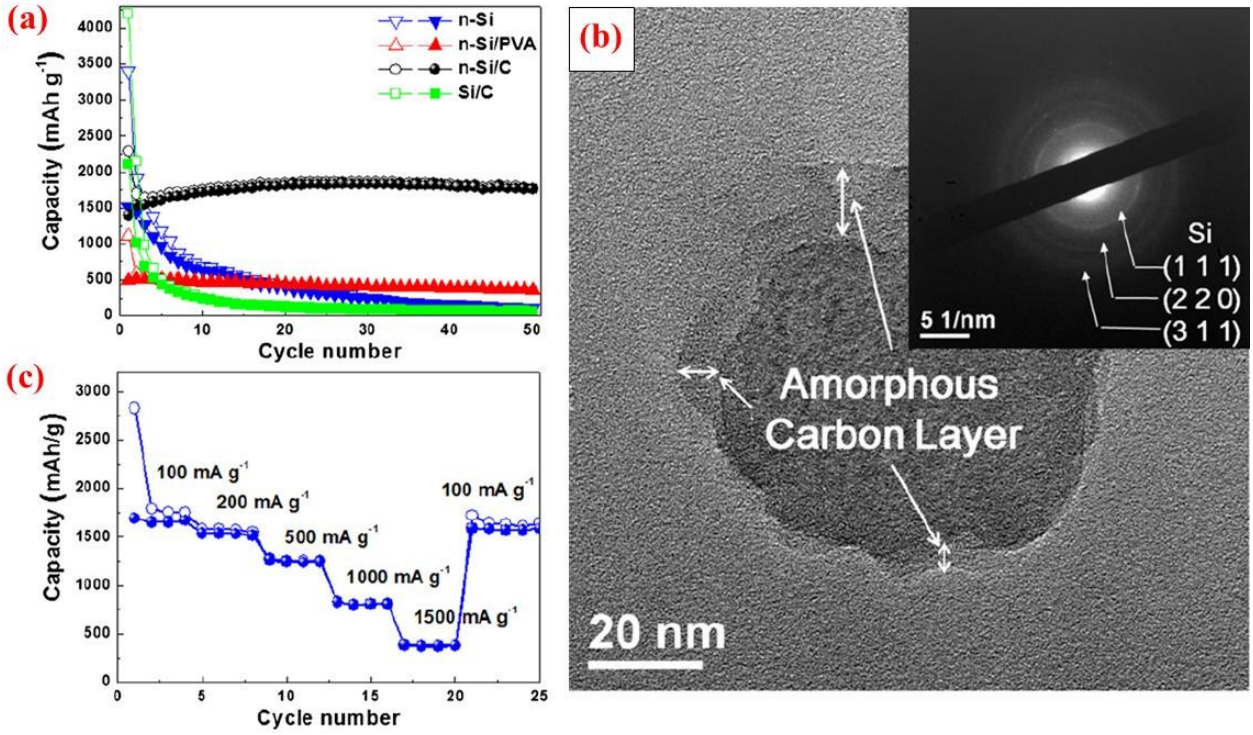

Figure 7. (a) Comparison of cyclability of n-Si, n-Si/PVA and n-Si/C electrodes at the constant current of 100 mA g^{-1}, (b) TEM image with SAED of n-Si/C of the 20th cycle at fully charge state to 1.5 V, and (c) rate capability test of n-Si/C electrode at the various current rates. Reproduced with permission[70] © 2012, Elsevier.

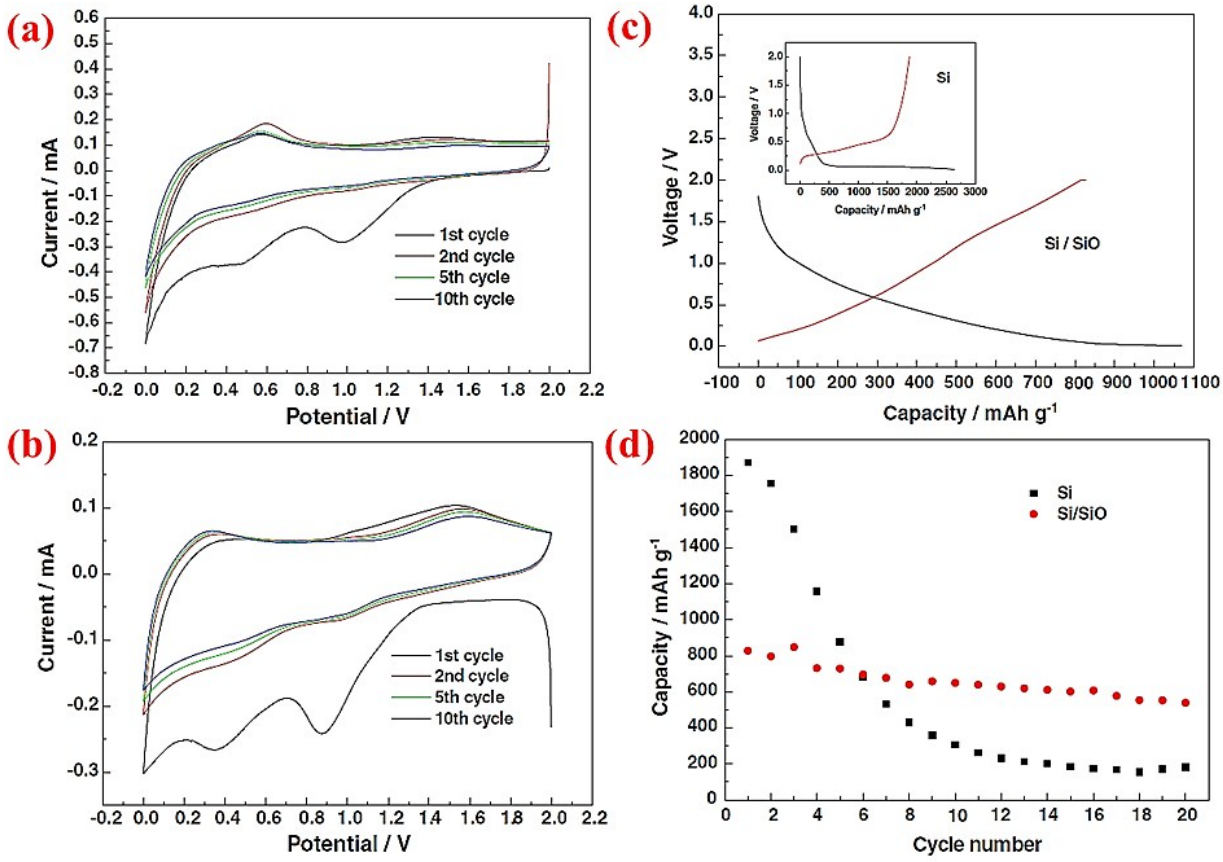

Figure 8. (a) CV curve for pure Si nanoparticles, (b) Si/SiO nanocomposite CV plot, (c) first charge/discharge profile of Si and core-shell Si/SiO nanomaterial, and (d) discharge capacity of nano-Si compared to Si/SiO composite for 20 cycles. Reproduced with permission[72] © 2007, Elsevier.

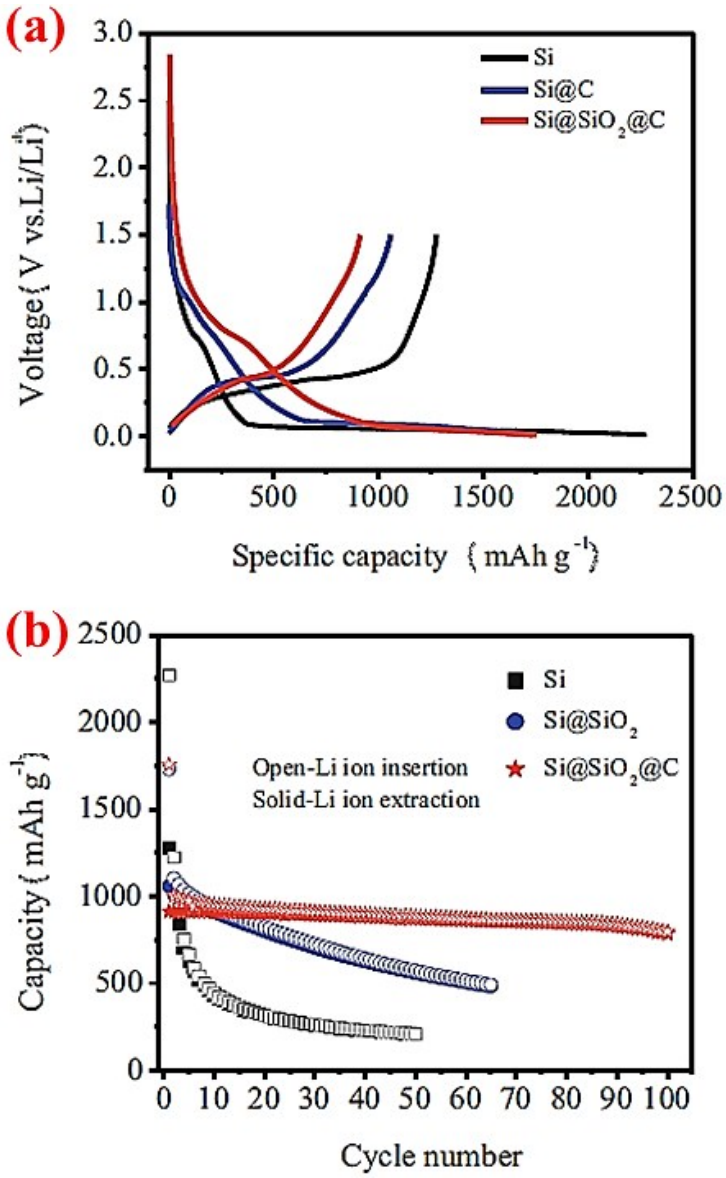

Figure 9. Cycling performance of double-walled core-shell structured Si@SiO_2@C composites. Reproduced with permission[43] © 2014, Springer.

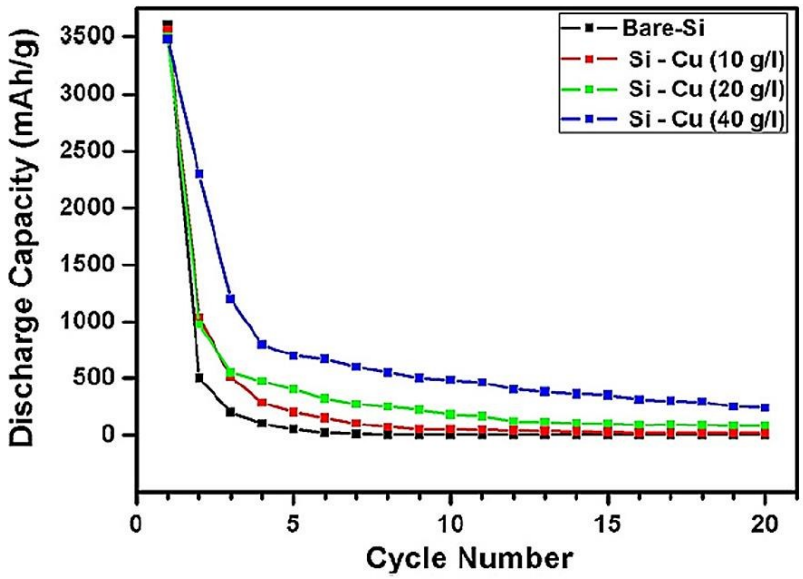

Figure 10. Cycling performance of copper coated silicon particles at different precursor concentrations in contrast to bare silicon particles. Reproduced with permission[44] © 2014, Elsevier.

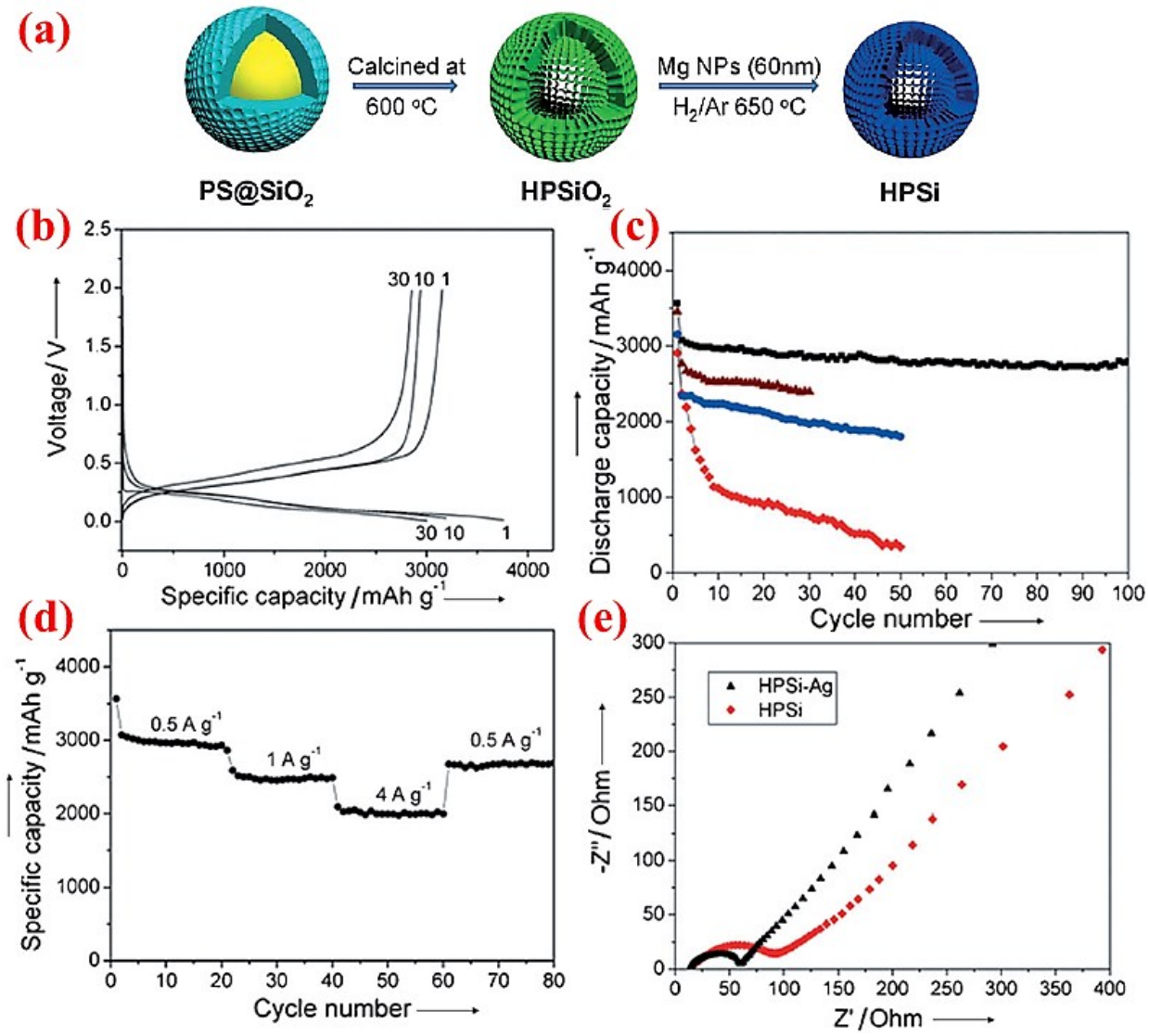

Figure 11. (a) Schematic of fabrication of the hollow porous Si (HPSi) nanostructure, (b) charge and discharge profile (measured vs. Li/Li^+) of HPSi@Ag nanoparticles, (c) HPSi@Ag nanocomposite (black), HPSi@C nanocomposite (brown), HPSi nanoparticles (blue), and commercial Si nanoparticles discharge capacities, (d) HPSi@Ag nanoparticles capacities at different charge rates, and (e) the Nyquist plot for HPSi and HPSi@Ag nanoparticles. Reproduced with permission[77] © 2012, Wiley-VCH Verlag.

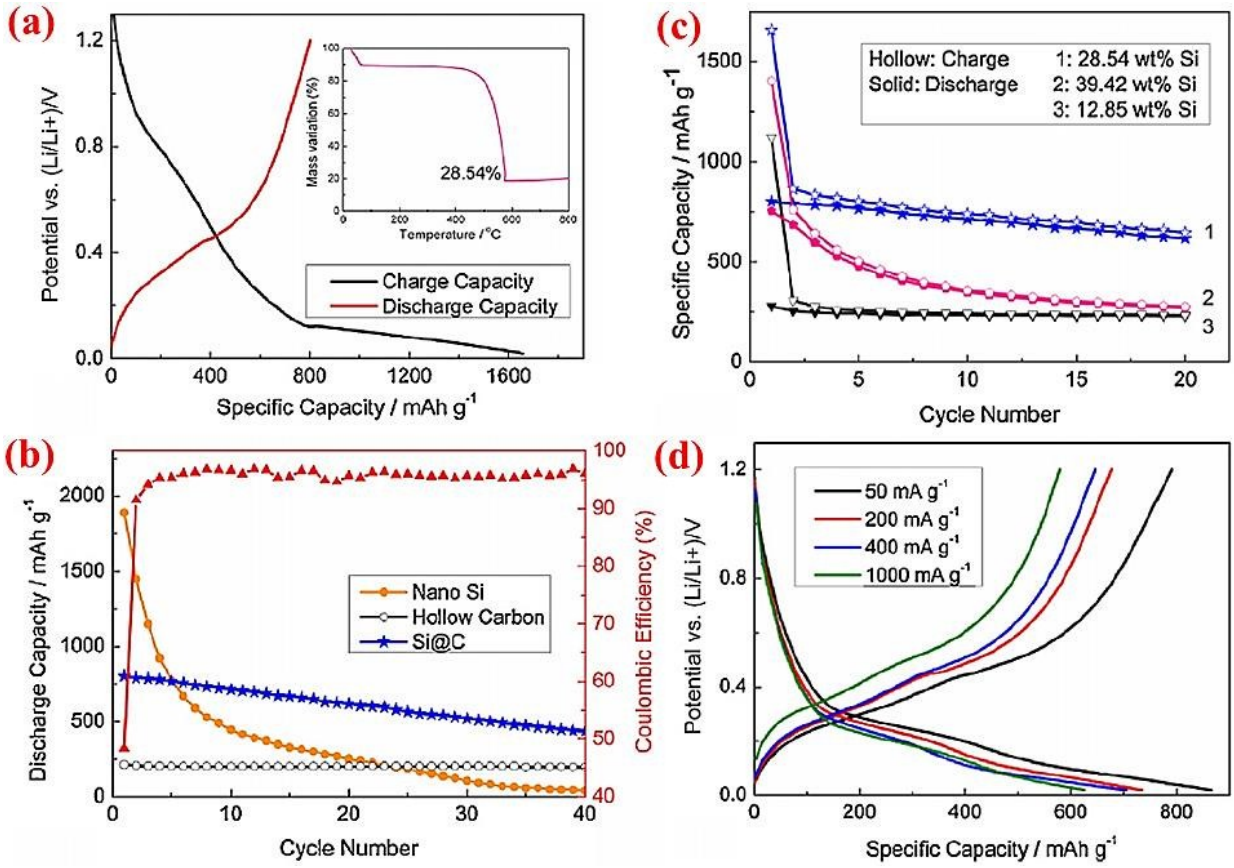

Figure 12. Electrochemical properties of the Si@C yolk-shell structure. Reproduced with permission[78] © 2013, Elsevier.

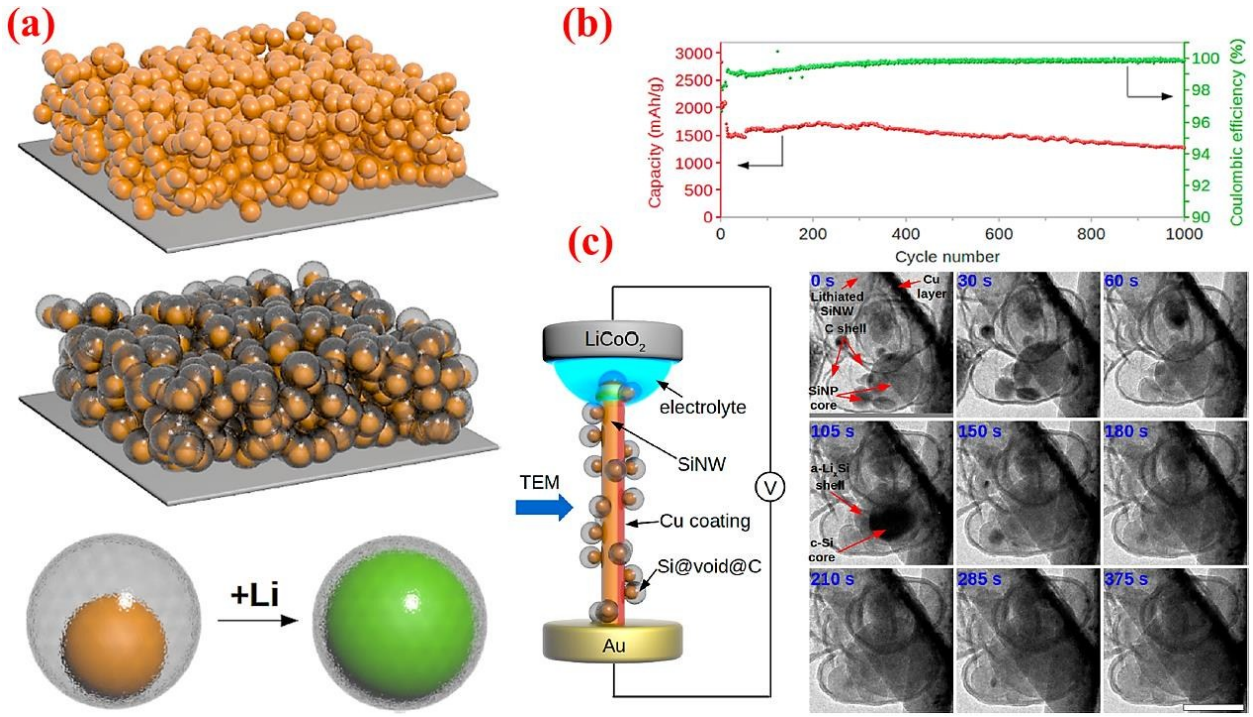

Figure 13. (a) schematic of yolk-shell silicon structure and how it can be lithiated, (b) cycling performance and coulombic efficiency of yolk-shell designed anodes, and (c) in situ TEM observations of lithiation process. Reproduced with permission[12] © 2012, American Chemical Society.

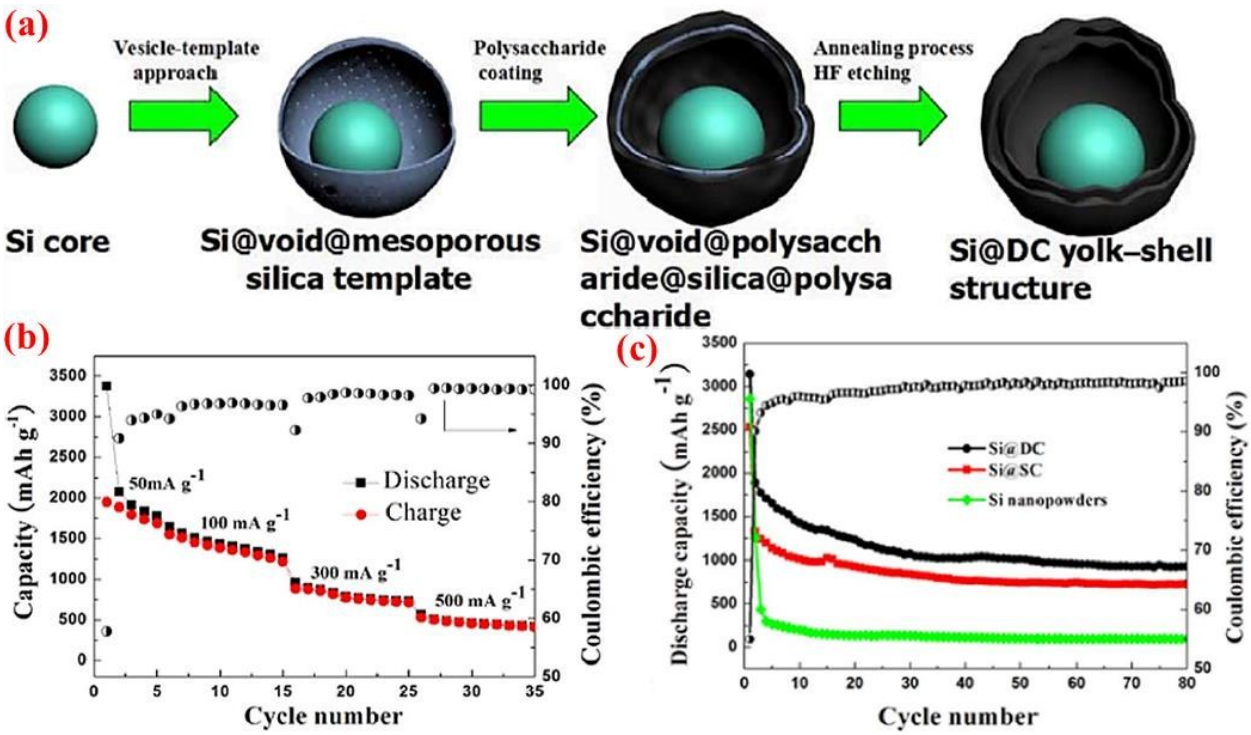

Figure 14. (a) Synthesis route of Si@DC based on the vesicle-template approach, (b) capacity retention curve at different current densities, (c) discharge capacity and coulombic efficiency of Si@DC nanoparticles in contrast with Si@SC and Si nanopowder. Reproduced with permission[46] © 2015, The Electrochemical Society.

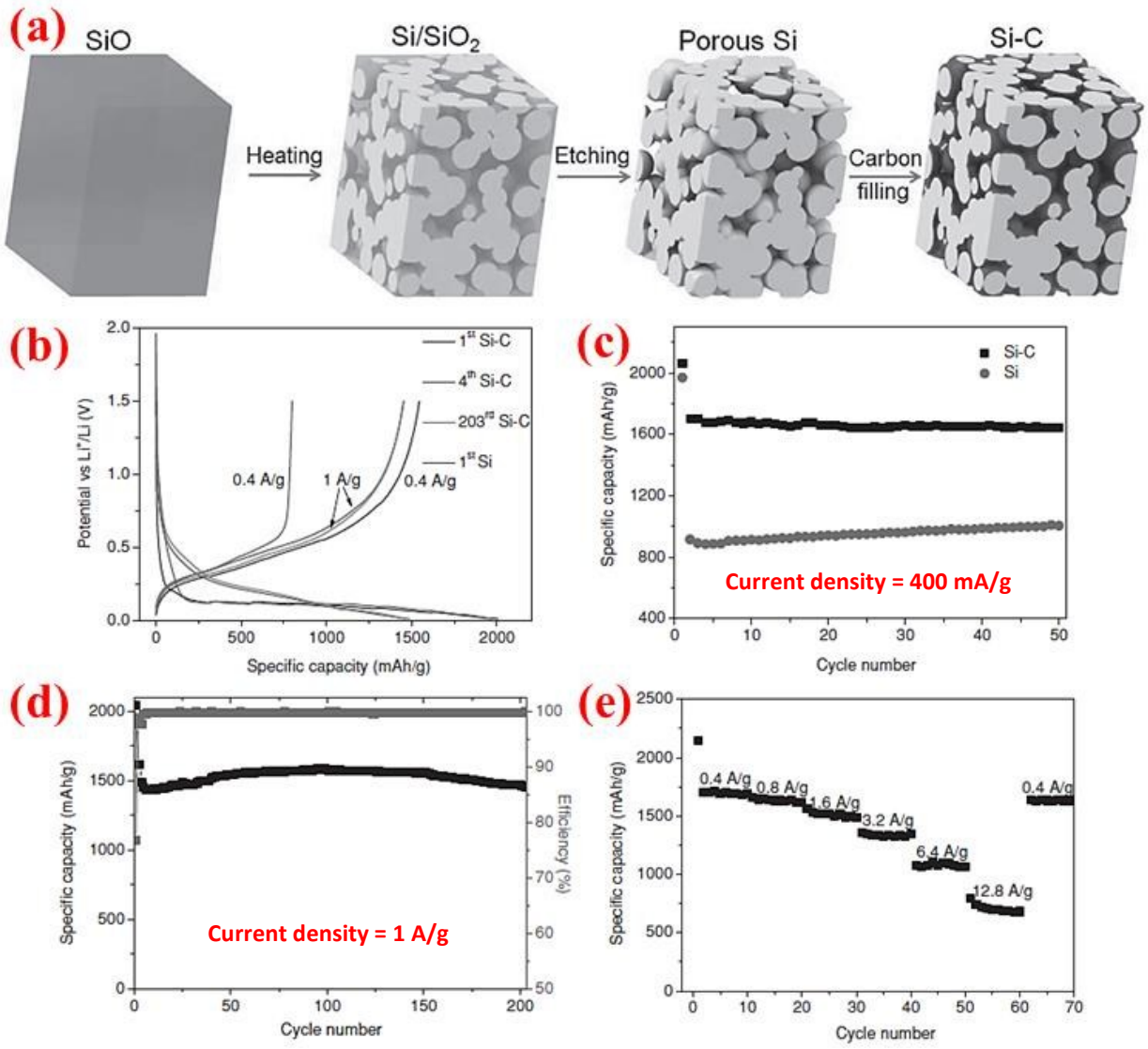

Figure 15. (a) Schematic of the synthesis procedure of micron-sized porous Si/C composites, and (b-e) electrochemical performance. Reproduced with permission[16] © 2013, Wiley-VCH Verlag.

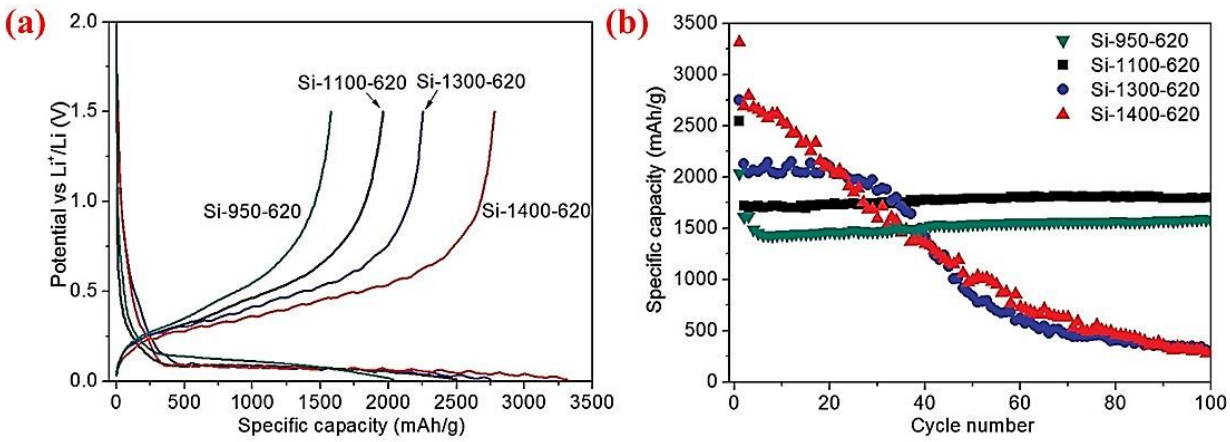

Figure 16. (a) First cycle discharge capacity, (b) cycling performance curves, of the micro-sized porous Si/C materials synthesized at different disproportionation temperatures. Reproduced with permission[80] © 2013, Wiley-VCH Verlag.

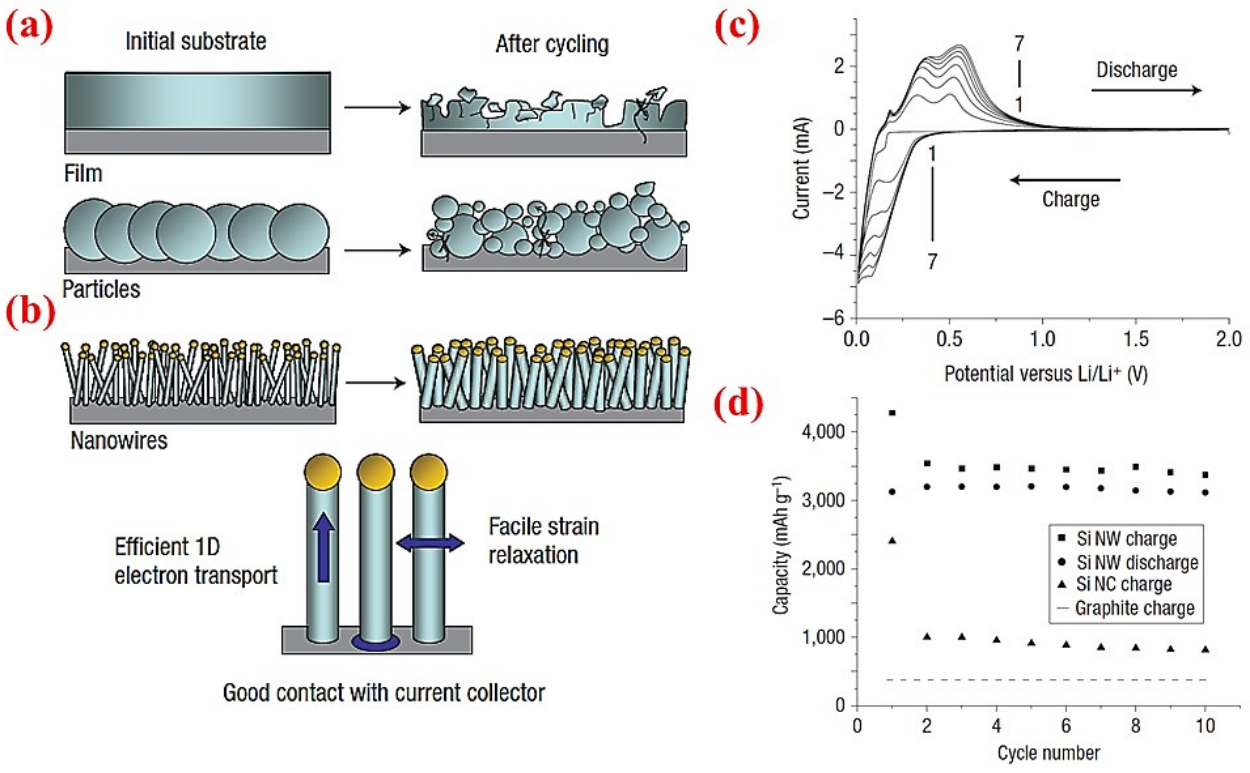

Figure 17. Comparison between morphology change of (a) silicon particles and (b) silicon nanowires after cycling, (c) CV data for SiNWs for 7 cycles, (d) comparison between the electrochemical performance of SiNWs, silicon nanocrystals (SiNCs) and graphite after 10 cycles. Reproduced with permission[4] © 2008, Nature Publishing Group.

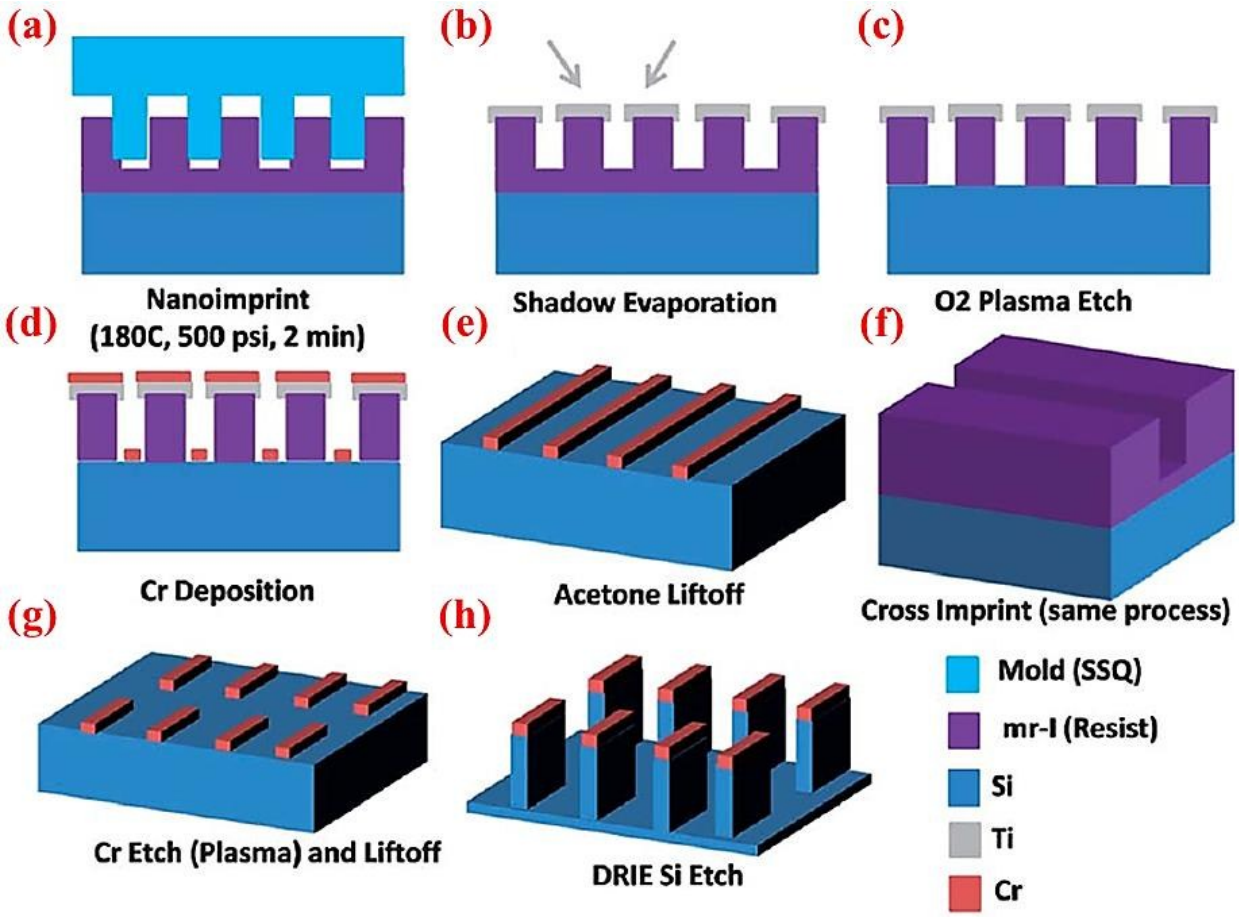

Figure 18. Schematic of multiple steps of NIL process to obtain SiNWLs. Reproduced with permission[47] © 2014, The Royal Society of Chemistry.

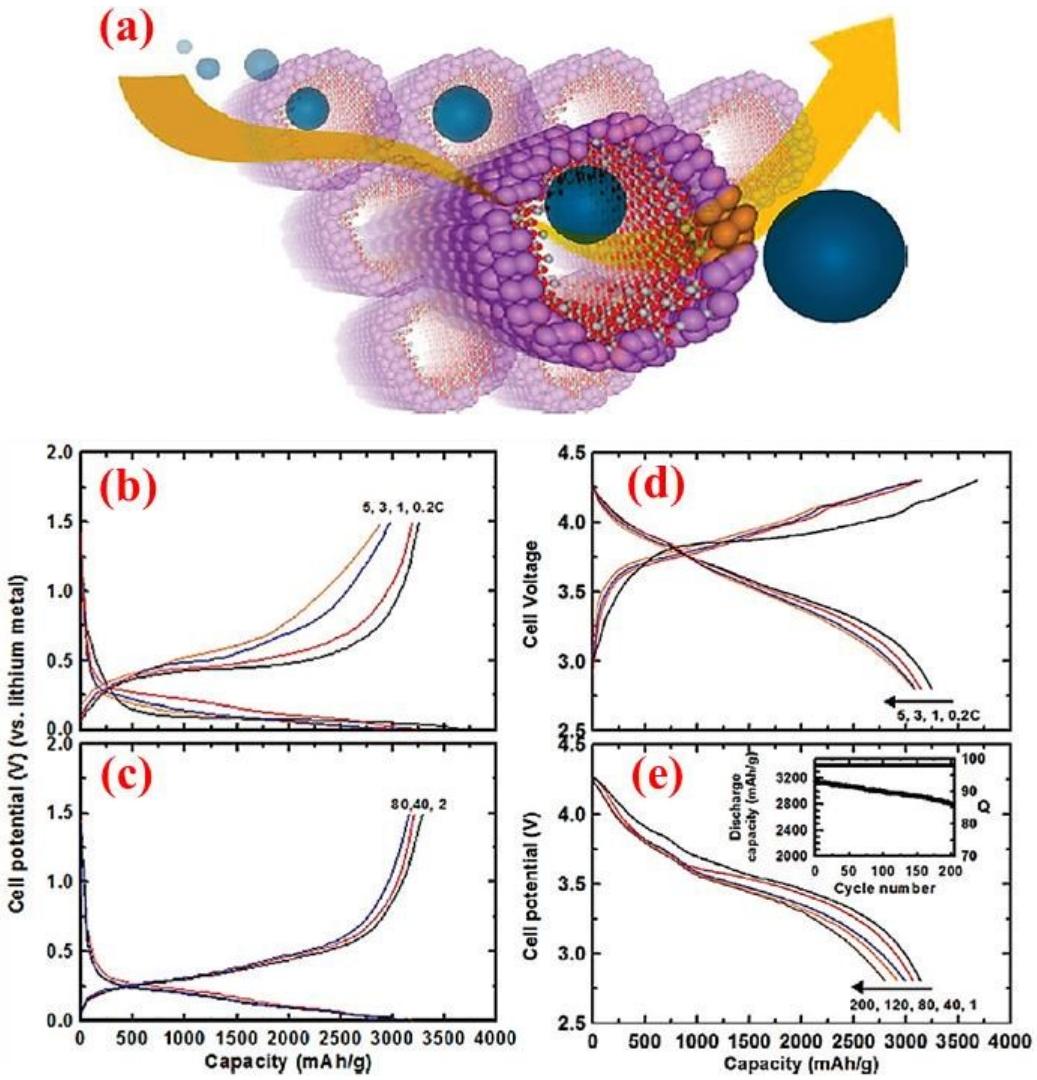

Figure 19. (a) Simulated pathways of Li ions in SiNTs, (b-c) voltage profiles of the coin-type half cells at charge rate of 1C and discharge rate ranging from 0.2C to 5C; and (d-e) voltage profiles of the pouch-type full cells ($LiCoO_2$ was cathode) for 200 cycles. Reproduced with permission[87] © 2009, American Chemical Society.

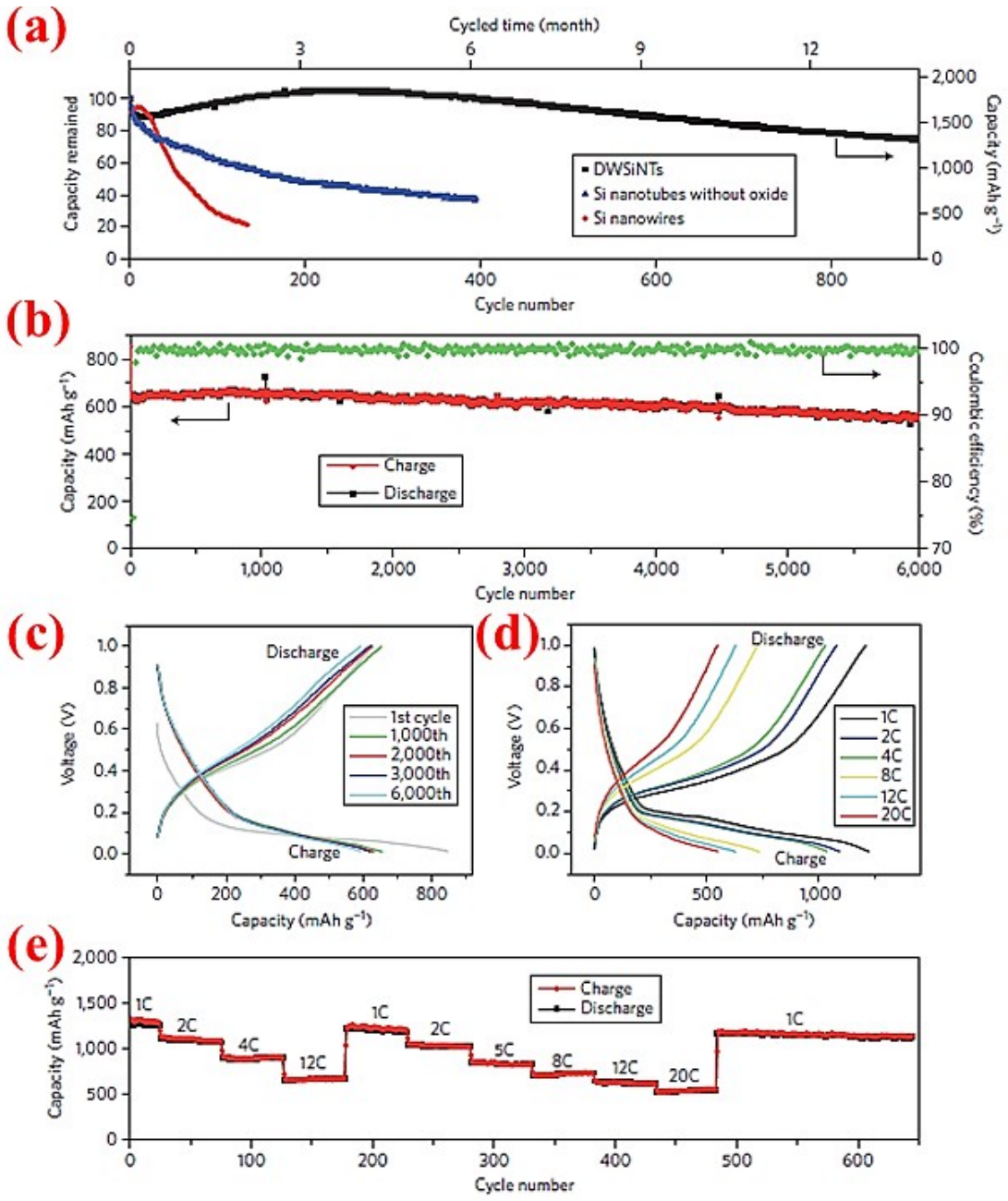

Figure 20. (a) Comparison in the capacity retention over cycles between DWSiNT and SiNWs at C/5; (b) capacity plot of DWSiNT anodes for 6000 cycles at 12C; (c) voltage vs. capacity plot for each 1000 cycles; (d) and (e) lithiation/delithiation profiles at different C-rates for multiple cycles. Reproduced with permission[89] © 2012, Nature Publishing Group.

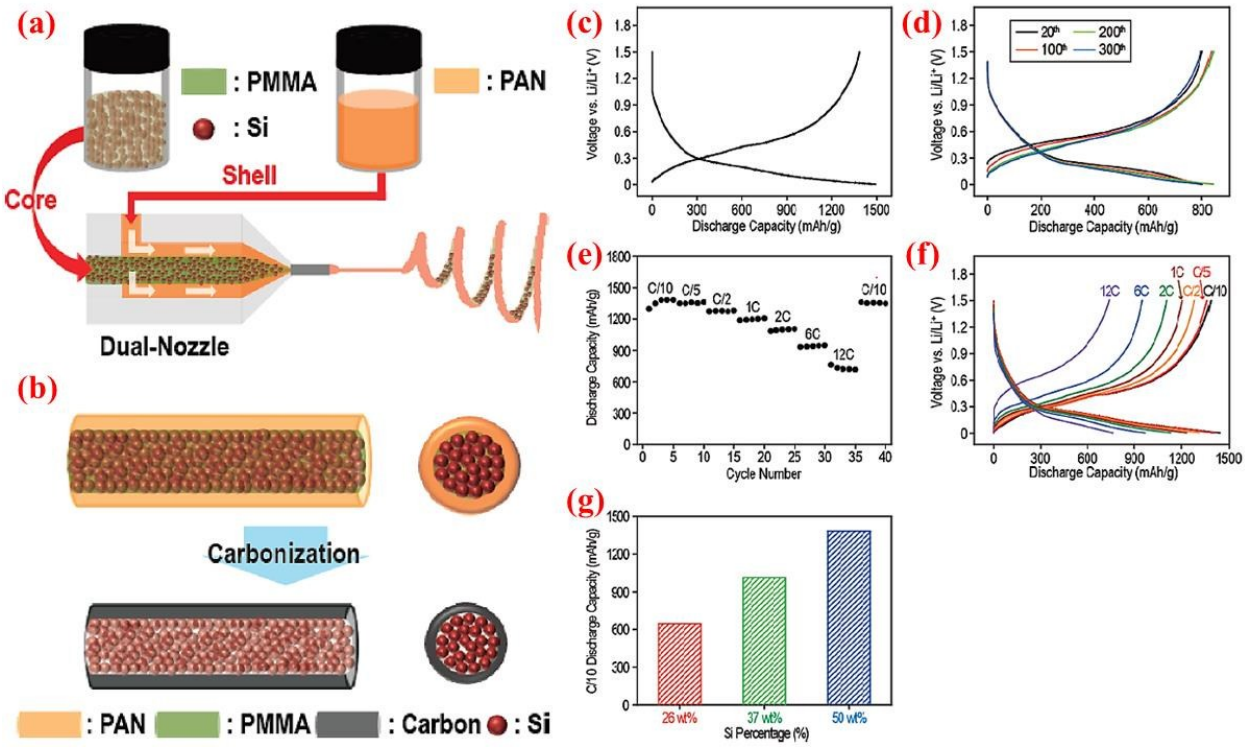

Figure 21. Core-shell nanofibers produced by (a) dual nozzle electrospinning machine, followed by (b) the carbonization step, (c-f) electrochemical performance, and (g) discharge capacity (measured at C/10 rate) vs. weight portion of silicon. Reproduced with permission[91] © 2011, American Chemical Society.

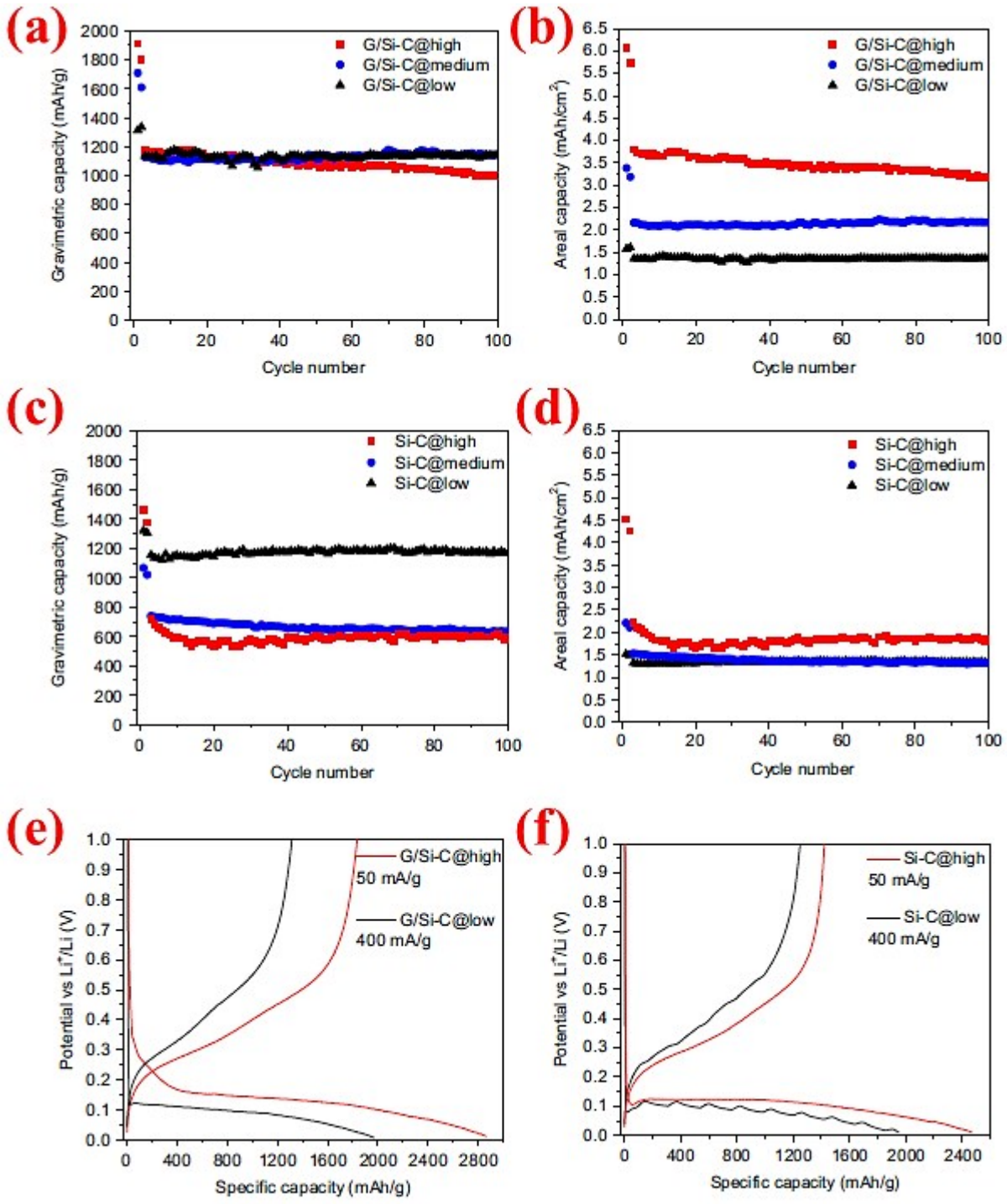

Figure 22. (a-d) Comparison between the cycling behavior of graphene/Si-C and Si-C composites at different mass loadings, (e-f) voltage profile of G/Si-C and Si-C composites for the first cycle at high and low mass loadings. Reproduced with permission[95] © 2014, Elsevier.

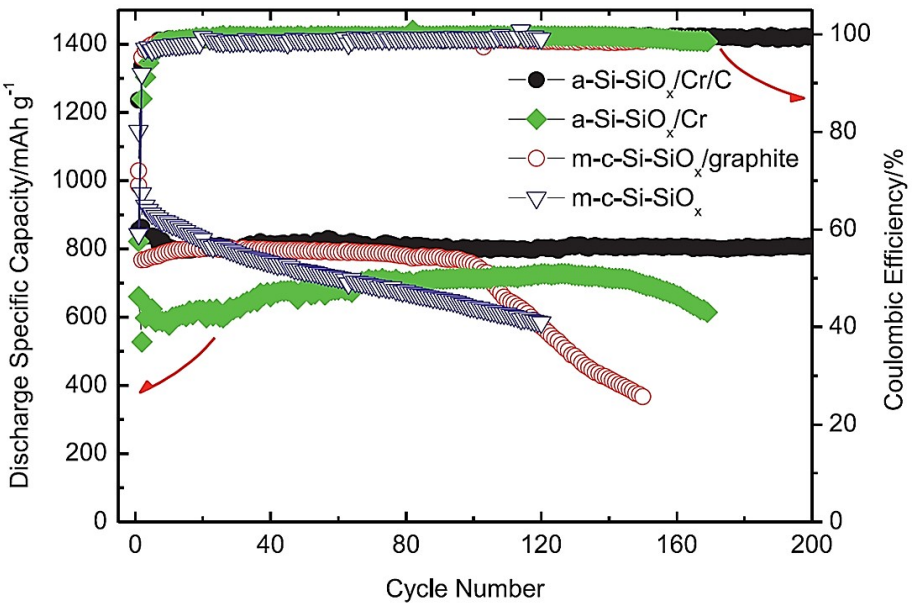

Figure 23. Comparison between specific discharge capacity of SiO/graphite, c-Si-SiOx/graphite, a-Si@SiOx/Cr and a-Si@SiOx/Cr/C vs. cycle number. Reproduced with permission[20] © 2015, Elsevier.

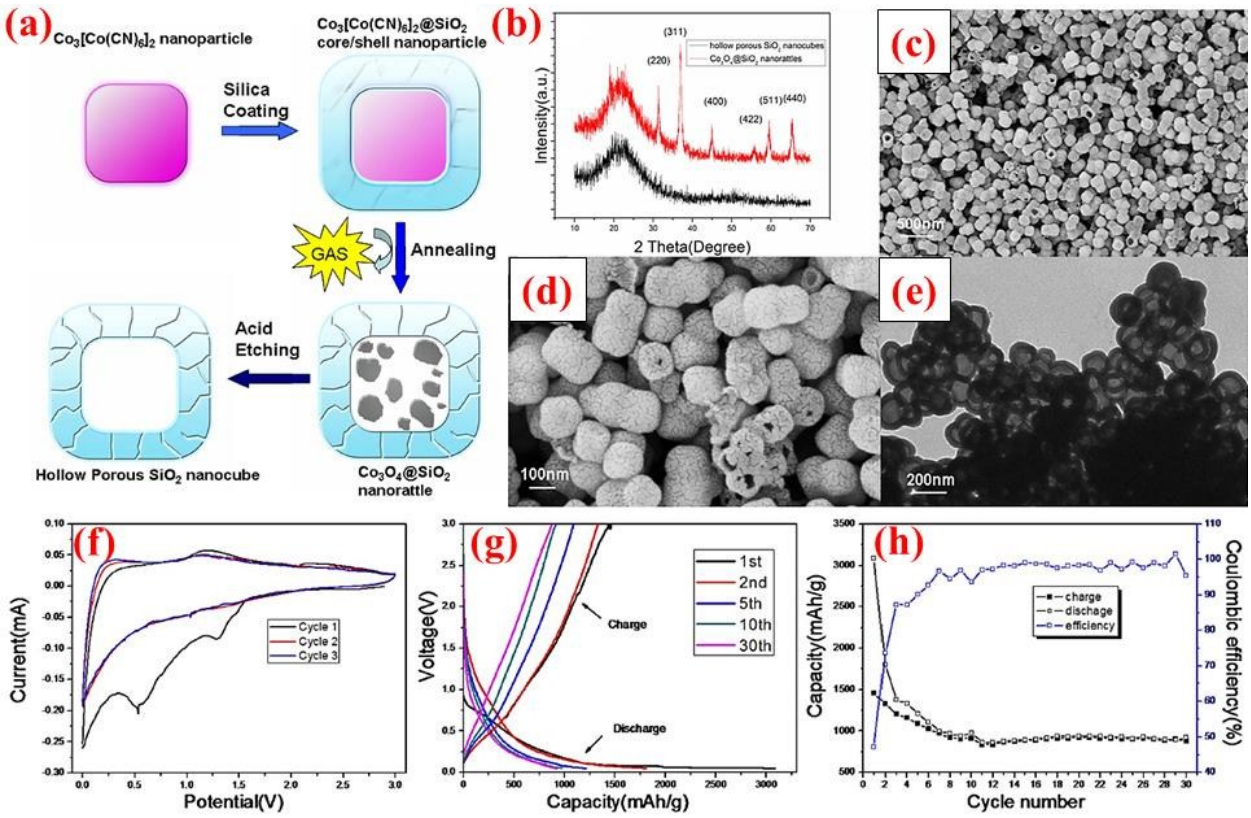

Figure 24. (a) Synthesis route of silica nanocubes; (b) XRD pattern, (c-d) SEM images, (e) TEM image, and (f-h) electrochemical data. Reproduced with permission[99] © 2013, Nature Publishing Group.

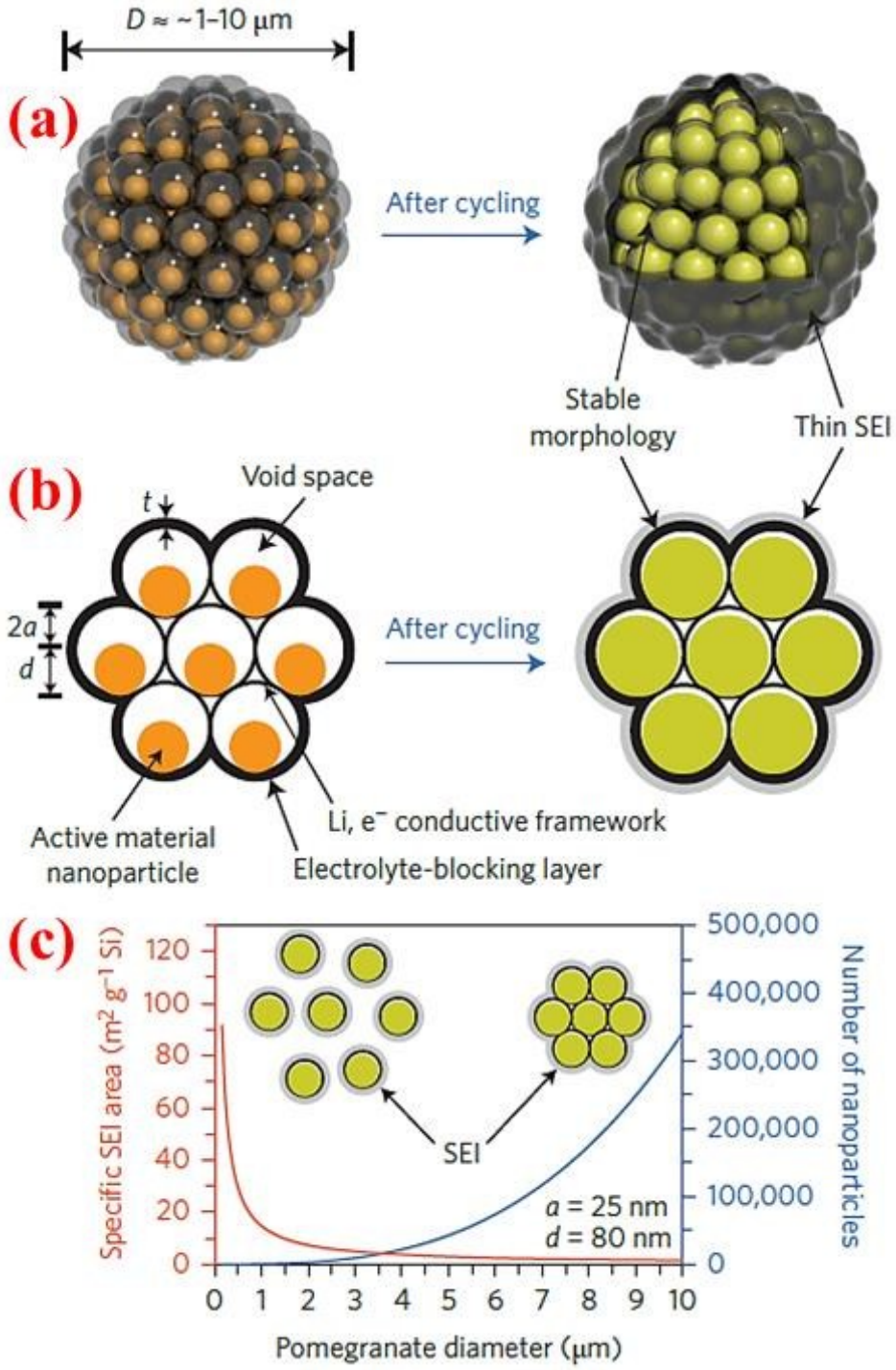

Figure 25. (a-b) Pomegranate design in both 3D and cross section views, (c) specific surface area in contact with electrolyte and number of particles vs. pomegranate diameter. Reproduced with permission[15] © 2014, Nature Publishing Group.

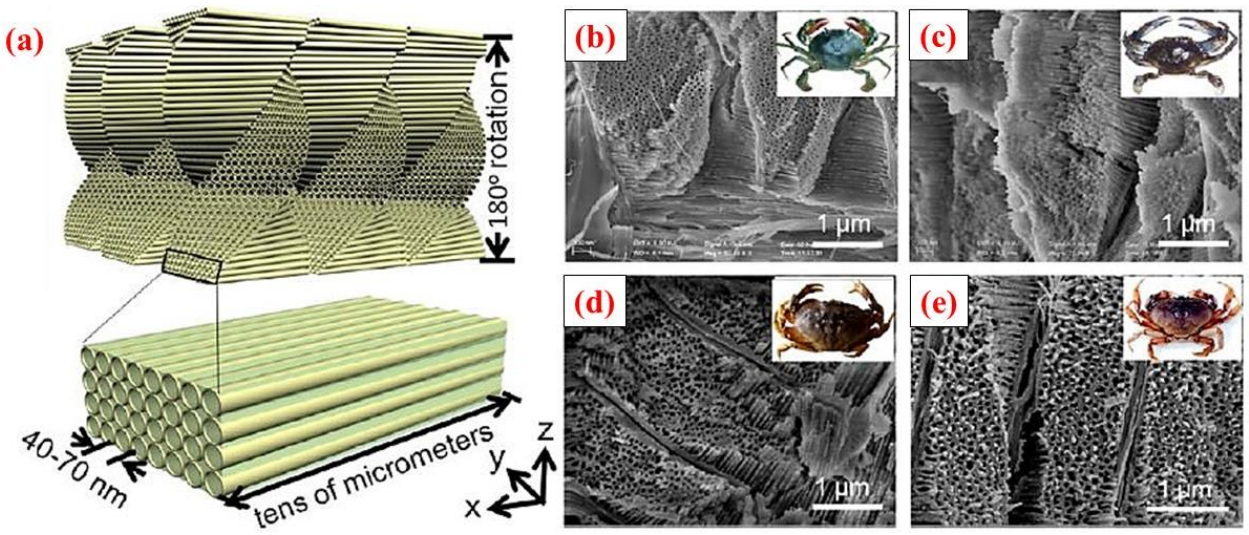

Figure 26. (a) Hollow nanochannles formed after removal of the organic fibers, (b-e) comparison between biotemplates prepared from different types of crab shells (Chinese hairy crab, blue crab, stone crab, and a Dungeness crab). Reproduced with permission[100] © 2013, American Chemical Society.